iScience

CellPress
OPEN ACCESS

Article

Bacterial surface properties influence the activity of the TAT-RasGAP$_{317-326}$ antimicrobial peptide

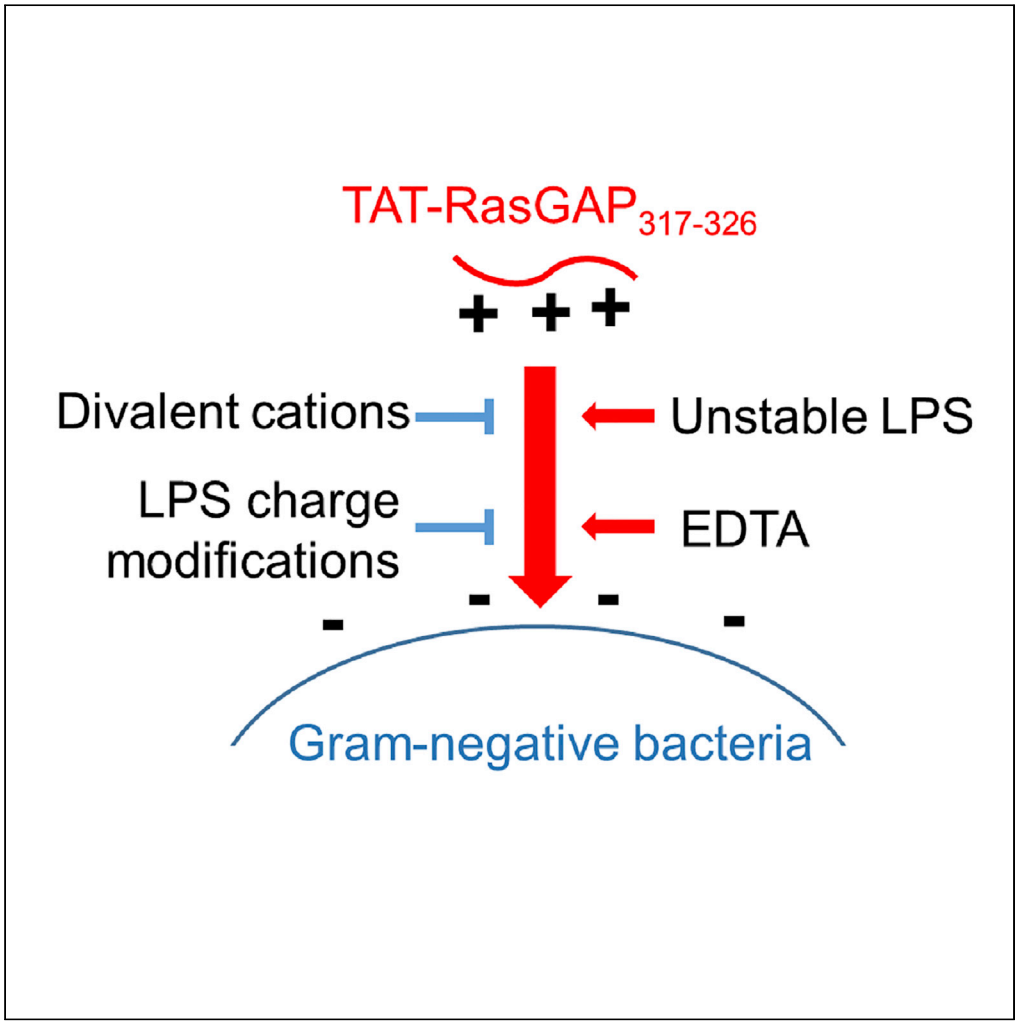

Maria Georgieva, Tytti Heinonen, Alessandra Vitale, ..., Leo Eberl, Christian Widmann, Nicolas Jacquier

christian.widmann@unil.ch (C.W.)
nicolas.jacquier@chuv.ch (N.J.)

Highlights

Antimicrobial activity of TAT-RasGAP$_{317-327}$ is affected by medium composition

Peptide exposure induces metabolic and stress responses

Cell surface modifications influence peptide antimicrobial activity

Resistance to TAT-RasGAP$_{317-327}$ peptide does not lead to multidrug resistance

Georgieva et al., iScience *24*, 102923
August 20, 2021
https://doi.org/10.1016/j.isci.2021.102923

iScience

CellPress
OPEN ACCESS

Article

Bacterial surface properties influence the activity of the TAT-RasGAP$_{317-326}$ antimicrobial peptide

Maria Georgieva,[2,4] Tytti Heinonen,[1,4] Alessandra Vitale,[3] Simone Hargraves,[1] Senka Causevic,[1] Trestan Pillonel,[1] Leo Eberl,[3] Christian Widmann,[2,*] and Nicolas Jacquier[1,5,*]

SUMMARY

Antibiotic resistance is an increasing threat for public health, underscoring the need for new antibacterial agents. Antimicrobial peptides (AMPs) represent an alternative to classical antibiotics. TAT-RasGAP$_{317-326}$ is a recently described AMP effective against a broad range of bacteria, but little is known about the conditions that may influence its activity. Using RNA-sequencing and screening of mutant libraries, we show that *Escherichia coli* and *Pseudomonas aeruginosa* respond to TAT-RasGAP$_{317-326}$ by regulating metabolic and stress response pathways, possibly implicating two-component systems. Our results also indicate that bacterial surface properties, in particular integrity of the lipopolysaccharide layer, influence peptide binding and entry. Finally, we found differences between bacterial species with respect to their rate of resistance emergence against this peptide. Our findings provide the basis for future investigation on the mode of action of TAT-RasGAP$_{317-326}$, which may help developing antimicrobial treatments based on this peptide.

INTRODUCTION

The spread of antibiotic resistance in many bacterial species is severely limiting the benefits of antibiotics and a growing number of infections are becoming harder to treat (O'Neill, 2016). Therefore, there is a need for new antimicrobials that could be used in the treatment of bacterial infections. Antimicrobial peptides (AMPs), several of which are already in clinical trials with promising results, represent a large source of antibacterial agents (Kumar et al., 2018). They are attractive alternatives to classical antibiotics due to their broad-spectrum activity that allows the targeting of a wide variety of bacterial species (Di Somma et al., 2020). In addition, AMPs have a relatively simple structure that can be bioengineered to increase, for example, their stability under physiological conditions or their resistance to degradation by gastrointestinal tract enzymes after oral administration (Kong et al., 2020).

AMPs were first described as naturally occurring peptides produced by many different organisms. Thousands have been identified (Wang et al., 2016; Kumar et al., 2018). In bacteria, AMP-producing strains have an advantage over other strains or species during competitive colonization of ecological niches (Hassan et al., 2012). In multicellular organisms, AMPs such as the human cathelicidin LL-37 and the bovine bactenecin are part of the innate immune system involved in the destruction of various microorganisms (Gennaro et al., 1989; Xhindoli et al., 2016).

Despite their diversity, AMPs share a number of common features: they are short peptides rich in cationic and hydrophobic amino acids and display an overall positive charge. To exert their biological activity, positively charged AMPs first interact with the negatively charged bacterial surface through electrostatic interactions (Brogden, 2005). This initial interaction with the bacterial surface is followed, for a majority of AMPs described up to date, by permeabilization and disruption of the membrane bilayer resulting in bacterial death. For example, this mechanism of killing has been demonstrated for melittin isolated from bee venom (Hong et al., 2019), human cathelicidin LL-37 (Mendez-Samperio, 2010), and polymyxin B derived from the Gram-positive bacterium *Bacillus polymyxa* (Srinivas and Rivard, 2017; Kumar et al., 2018).

TAT-RasGAP$_{317-326}$ is a recently identified AMP showing antimicrobial and antibiofilm activities *in vitro* (Heulot et al., 2017; Heinonen et al., 2021). This peptide is composed of a cell permeable moiety, the TAT HIV 48–57 sequence, and a 10 amino acid sequence derived from the Src homology 3 domain of p120 RasGAP.

[1]Institute of Microbiology, Lausanne University Hospital and University of Lausanne, Lausanne 1011, Switzerland

[2]Department of Biomedical Sciences, University of Lausanne, Lausanne 1005, Switzerland

[3]Department of Plant and Microbial Biology, University of Zurich, Zurich 8008, Switzerland

[4]These authors contributed equally

[5]Lead contact

*Correspondence: christian.widmann@unil.ch (C.W.), nicolas.jacquier@chuv.ch (N.J.)

https://doi.org/10.1016/j.isci.2021.102923

Table 1. *E. coli* MG1655, ATCC25922, and *P. aeruginosa* PA14 sensitivity to TAT-RasGAP$_{317-326}$ varies depending on the growth medium used

		TAT-RasGAP$_{317-326}$		Polymyxin B	
Strain	Medium	MIC (μM)	IC_{50} (μM)	MIC (μg/mL)	IC_{50} (μg/mL)
E. coli MG1655	LB	8	3	1	0.6
	LB Mg^{high}	32	16.3	2	0.6
	BM2 Mg^{low}	0.5	0.3	2	1.0
	BM2 Mg^{high}	4	2	2	0.8
E. coli ATCC 25922	LB	8	5.2	2	1.8
	LB Mg^{high}	128	52	4	2.7
P. aeruginosa PA14	LB	32	7.2	4	2.1
	LB Mg^{high}	64	20.8	2	1.0
	BM2 Mg^{low}	4	1.7	4	1.0
	BM2 Mg^{high}	32	10.1	1	0.5

The indicated strains were grown overnight in LB, LB with 2 mM $MgSO_4$ (LB Mg^{high}), BM2 with 20 μM $MgSO_4$ (BM2 Mg^{low}), or BM2 with 2 mM $MgSO_4$ (BM2 Mg^{high}). Culture was then diluted to OD_{600} = 0.1 and grown for 1 hr. Bacterial suspension was further diluted 20 times for *E. coli* and 10 times for *P. aeruginosa* and 10 μL was added per well of a 96-well plate containing 100 μl of serial dilutions of TAT-RasGAP$_{317-326}$ or polymyxin B. OD_{590} was measured after 16 hr of incubation. MIC is defined as the lowest concentration of TAT-RasGAP$_{317-326}$ that completely inhibits bacterial proliferation. IC_{50} is defined as the concentration required to inhibit 50% of growth and was calculated using GraphPad Prism 8. The detailed growth curves are presented in Figures S2–S4.

TAT-RasGAP$_{317-326}$ is 22 amino acid long, with a molar mass of 2830 g/mol and a net charge of +9 at pH 7.0. In comparison, melittin is 26 amino acid long, with a molar mass of 2847 g/mol and a net charge of +6 at pH 7.0 and polymyxin B is a mixture of highly similar cationic peptides composed of a non-ribosomal cyclic heptapeptide with a tripeptide side chain (molar mass of 1302 g/mol) (Figure S1) (Yang et al., 2001; Velkov et al., 2013; Hong et al., 2019). TAT-RasGAP$_{317-326}$ was initially identified as an anticancer compound that sensitizes cancer cells to genotoxins (Michod et al., 2004, 2009) and to radiotherapy (Tsoutsou et al., 2017). This peptide also inhibits cell migration and invasion (Barras et al., 2014c) and possesses anti-metastatic activity *in vivo* (Barras et al., 2014b). It can also directly lyse a subset of cancer cells by targeting plasma membrane inner leaflet-enriched phospholipids (Serulla et al., 2020) in a manner that does not involve known programmed cell death pathways (Annibaldi et al., 2014; Heulot et al., 2016). We have previously shown that the tryptophan residue at position 317 of the TAT-RasGAP$_{317-326}$ peptide is essential for its activity against both eukaryotic and bacterial cells (Barras et al., 2014a; Heulot et al., 2017). TAT-RasGAP$_{317-326}$ minimal inhibitory concentrations (MICs) were relatively low against *Escherichia coli* and *Acinetobacter baumannii* (11 μM and 2.9 μM respectively) and higher against *Pseudomonas aeruginosa* and *Staphylococcus aureus* (23 μM and 46 μM respectively), indicating that different bacterial species have different levels of tolerance toward this peptide (Heulot et al., 2017). In addition, TAT-RasGAP$_{317-326}$ showed limited protection in a mouse model of *E. coli*-induced peritonitis (Heulot et al., 2017). Physiological factors may have contributed to the poor biodistribution and rapid clearance of TAT-RasGAP$_{317-326}$ and, subsequently, to its low efficacy in this setting (Michod et al., 2009).

In this study, we assessed TAT-RasGAP$_{317-326}$ activity under various experimental settings to better characterize the peptide activity, as well as the bacterial response to peptide exposure. Our findings provide important initial insights into the activity of the TAT-RasGAP$_{317-326}$ peptide that will pave the way for further investigation on its antimicrobial properties.

RESULTS

Divalent cations reduce TAT-RasGAP$_{317-326}$ surface binding and entry into bacteria

P. aeruginosa grown under low Mg^{2+} conditions is resistant to EDTA, gentamicin, and polymyxin B via a mechanism that involves outer membrane modifications (Macfarlane et al., 1999; McPhee et al., 2003; Olaitan et al., 2014). To determine whether the antimicrobial activity of TAT-RasGAP$_{317-326}$ is also affected by Mg^{2+} levels, we assessed how Mg^{2+} modulated its MIC and concentration inhibiting growth by 50% (IC_{50}) in three laboratory strains, *E. coli* MG1655, *E. coli* ATCC 25922, and *P. aeruginosa* PA14. The results of these experiments are summarized in Table 1 and shown in detail in Figures S2–S4. The

MIC of TAT-RasGAP$_{317-326}$ in standard Luria-Bertani (LB) medium for *E. coli* and *P. aeruginosa* was determined to be 8 μM and 32 μM (corresponding to 22.63 μg/ml and 90.56 μg/ml), respectively. There was a small difference in peptide MIC levels between LB and BM2 medium supplemented with 2 mM $MgSO_4$ (BM2 Mg^{high}) for both *E. coli* and *P. aeruginosa*. However, these two bacterial species displayed an 8-fold decrease in MIC of TAT-RasGAP$_{317-326}$ in BM2 containing 20 μM $MgSO_4$ (BM2 Mg^{low}) relative to 2 mM $MgSO_4$ (BM2 Mg^{high}). MIC of polymyxin B in BM2 Mg^{high} toward *E. coli* and *P. aeruginosa* was measured as 2 μg/ml and 1 μg/ml (1.66 μM and 0.83 μM), respectively. Low magnesium in BM2 medium resulted in a 4-fold increase of MIC of polymyxin B in *P. aeruginosa* but had no impact in *E. coli*. Our results agree with earlier data that low Mg^{2+} increases *P. aeruginosa* resistance to polymyxin B (Macfarlane et al., 1999; McPhee et al., 2003). Altogether, these findings show that low Mg^{2+} in culture medium renders bacterial cells more susceptible to TAT-RasGAP$_{317-326}$ but not to polymyxin B.

Because BM2 is a defined bacteriological medium, we also investigated whether Mg^{2+} affects the sensitivity to TAT-RasGAP$_{317-326}$ in complex medium such as LB. We compared peptide MIC in LB and LB supplemented with 2 mM $MgSO_4$ (LB Mg^{high}) and found that high Mg^{2+} increased peptide MIC toward both *E. coli* and *P. aeruginosa* (Table 1), consistent with the data obtained with these two bacterial strains in BM2 medium. Moreover, the ability of TAT-RasGAP$_{317-326}$ to hamper *E. coli* growth rate was clearly inhibited by 2 mM $MgSO_4$ (Figures 1A and 1B). Therefore, high Mg^{2+} levels decreased bacterial sensitivity to TAT-RasGAP$_{317-326}$ and this result was independent of the medium used. We also determined that the MIC of polymyxin B for *P. aeruginosa* decreased in the presence of high Mg^{2+} in LB (Table 1), which is in accordance with our data for *P. aeruginosa* in BM2 medium.

Would cations other than Mg^{2+} also render bacteria less sensitive to TAT-RasGAP$_{317-326}$? Addition of Fe^{2+} and Ca^{2+} in culture medium decreased the sensitivity of *E. coli* to peptide (Figures 1C and 1D). We also found that high Mg^{2+} concentrations decreased bacterial sensitivity to TAT-RasGAP$_{317-326}$ both in the context of sulfate and chloride counterions (Figures 1B and 1E). In contrast, ammonium sulfate did not affect bacterial susceptibility to TAT-RasGAP$_{317-326}$ (Figure 1F). Collectively, these results indicate that the Fe^{2+}, Ca^{2+} and Mg^{2+} divalent cations in culture medium both hamper the ability of TAT-RasGAP$_{317-326}$ to kill bacteria.

Since divalent cations are known to influence outer membrane characteristics, such as lipopolysaccharide (LPS) integrity (Hancock, 1997), we questioned whether TAT-RasGAP$_{317-326}$ binding and internalization were altered by these cations. Fe^{2+}, and to a lower extent Ca^{2+} and Mg^{2+}, decreased the levels of FITC-labeled TAT-RasGAP$_{317-326}$ bound to the surface of *E. coli,* as well as the amount of internalized peptide (Figure 1G). However, we found that peptide binding and internalization were not affected by ammonium sulfate – a finding that is consistent with our data that ammonium sulfate does not impact peptide MIC (Figure 1F). Altogether, these data suggest that divalent cations decrease bacterial sensitivity to TAT-RasGAP$_{317-326}$ peptide via a mechanism that restricts peptide binding and entry in bacteria.

TAT-RasGAP$_{317-326}$ is bactericidal against *E. coli* and *P. aeruginosa*

To determine the relationship between peptide exposure and the number of viable (culturable) bacteria, we performed colony formation unit (CFU) assays. For *E. coli* grown in LB, 10 μM of TAT-RasGAP$_{317-326}$ induced an initial 2- to 5- fold decrease in the number of surviving bacteria, but there was no further decrease upon longer incubation times (Figure 2A). A more pronounced decrease in bacterial viability was observed at peptide concentrations $\geq$15 μM, indicating that the peptide is bactericidal at these concentrations (Figure 2A). Confocal microscopy studies showed that *E. coli* accumulated TAT-RasGAP$_{317-326}$ intracellularly when exposed to a concentration leading to bacterial killing (Figure 2E). Furthermore, peptide exposure at this concentration led to changes in bacterial morphology as seen by electron microscopy (Figure 2F). For *P. aeruginosa* grown in BM2 Mg^{low} medium, 0.5–2 μM TAT-RasGAP$_{317-326}$ had a small impact on bacterial growth relative to the untreated control, while 5–10 μM strongly reduced bacterial numbers (Figure 2B). In order to analyze the kinetics of peptide activity at early time points, we performed survival curves using 20 μM of TAT-RasGAP$_{317-326}$ peptide for *E. coli* and 10 μM for *P. aeruginosa*. These concentrations correspond to 2.5 times the MIC of TAT-RasGAP$_{317-326}$ (Table 1) and were shown to kill a majority of bacteria (Figures 2A and 2B). We monitored bacterial killing for the first two hours of peptide exposure and compared bacterial killing by TAT-RasGAP$_{317-326}$ and polymyxin B; the latter also added at 2.5 times its MIC (2.5 μg/mL for *E. coli* and 10 μg/mL for *P. aeruginosa*). Interestingly, TAT-RasGAP$_{317-326}$ displayed slow time-kill kinetics in comparison to polymyxin B against *E. coli* (Figure 2C). In *P. aeruginosa*, however, the killing kinetics were similar between TAT-RasGAP$_{317-326}$ and polymyxin B (Figure 2D).

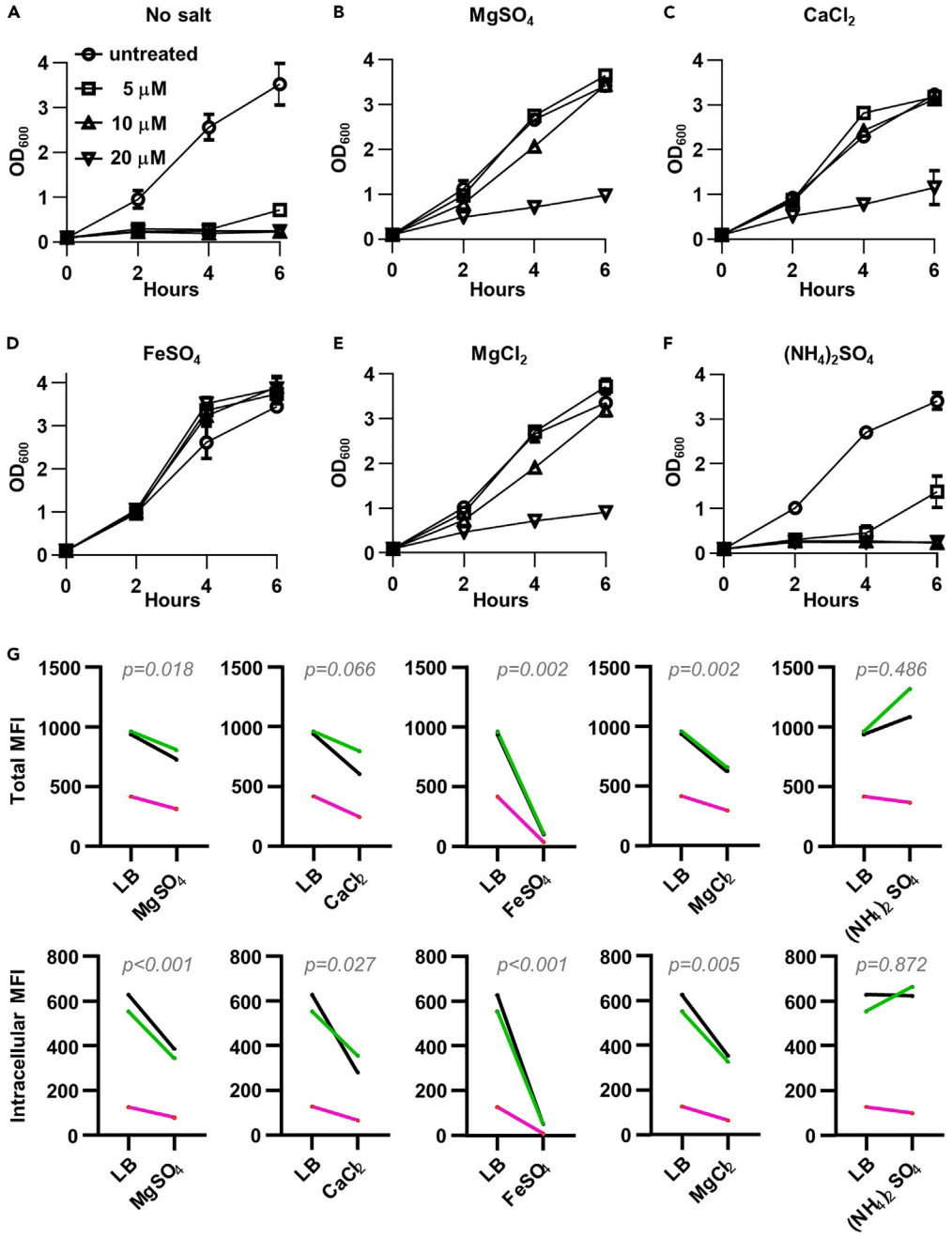

Figure 1. Divalent cations affect bacterial sensitivity toward TAT-RasGAP$_{317-326}$ and decrease binding and entry of the peptide in *E. coli*

(A–F) *E. coli* MG1655 were grown overnight at 37°C in LB supplemented with 2 mM of the indicated salt and diluted to OD_{600} = 0.1. Bacterial suspension was then grown 1 hr at 37°C before addition of the indicated concentrations of TAT-RasGAP$_{317-326}$. OD_{600} was measured at the indicated times after the initial dilution. The results correspond to the mean ± the range of two independent experiments.

(G) *E. coli* MG1655 were grown overnight at 37°C in LB containing 2 mM of the indicated salts and diluted to OD_{600} = 0.1. Bacterial binding and uptake of 10 μM FITC-labeled TAT-RasGAP$_{317-326}$ were recorded in three independent experiments (each shown with a different color on the graph) via flow cytometry with (Intracellular) or without (Total) quenching with 0.2% trypan blue. p values were calculated by ratio paired t test between the indicated condition and the LB control.

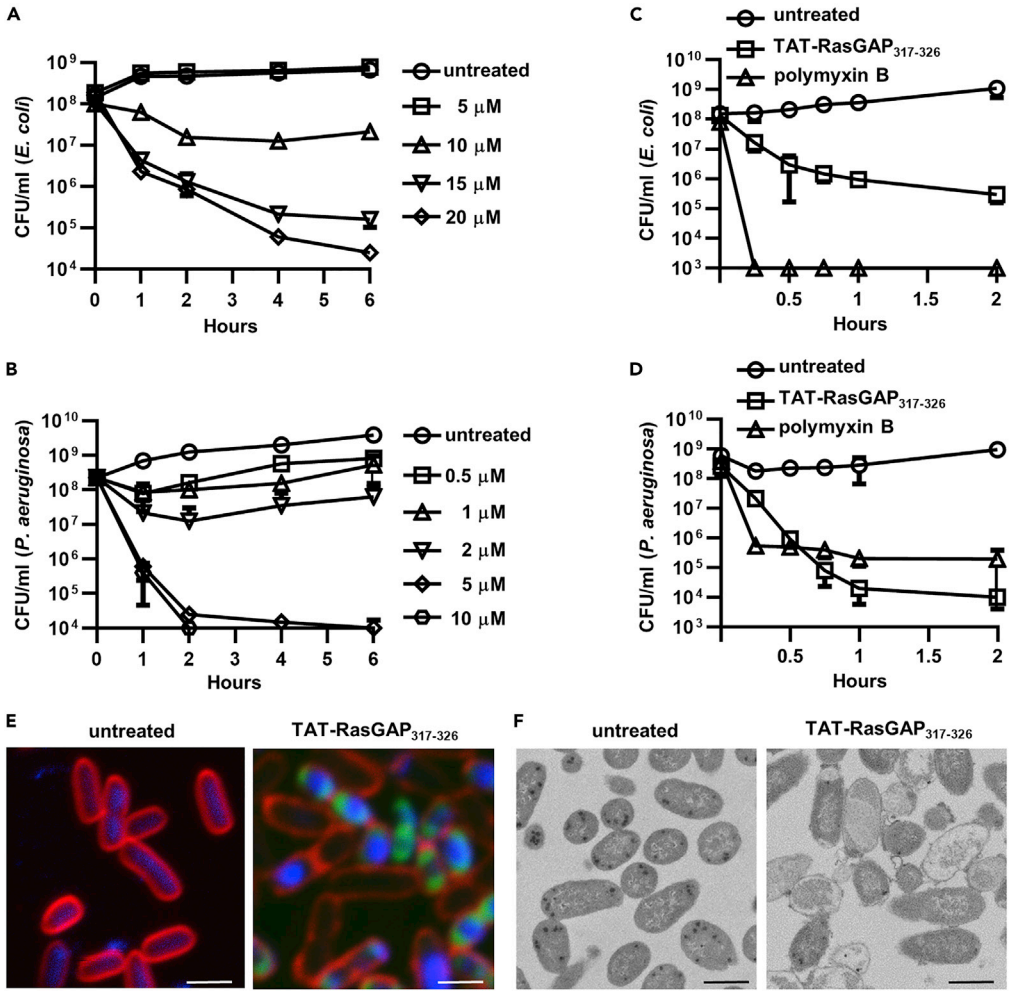

Figure 2. TAT-RasGAP$_{317-326}$ is bactericidal against *E. coli* and *P. aeruginosa*

(A and B) Overnight cultures of *E. coli* MG1655 in LB (A) and *P. aeruginosa* PA14 in BM2 Mg^{low} (B) were diluted to OD_{600} = 0.1 and incubated at 37°C for 1 hr. TAT-RasGAP$_{317-326}$ was then added at the indicated concentrations. Samples were taken at the indicated time points, serially diluted 10-fold in fresh LB and plated on LB agar plates. Number of colony forming units per ml (CFU/mL) in the original culture was calculated.

(C) *E. coli* cultures were treated as in (A). TAT-RasGAP$_{317-326}$ (20 μM) or polymyxin B (2.5 μg/mL) were added as indicated. Samples were taken at the indicated time points and CFU/ml were determined as in (A).

(D) *P. aeruginosa* cultures were treated as in (B). TAT-RasGAP$_{317-326}$ (10 μM) or polymyxin B (10 μg/mL) were added as indicated. Samples were taken at the indicated time points and CFU/ml were determined as in (A). (A–D): the results correspond to the mean ± standard deviation from at least two independent experiments.

(E) *E. coli* MG1655 grown overnight and diluted to OD_{600} = 0.1 were incubated for 1 hr with or without 20 μM FITC-labeled TAT-RasGAP$_{317-326}$ (green). The bacteria were then labeled with 5 μg/mL FM4-64 (red) and fixed with 4% paraformaldehyde. Incubation with DAPI (blue) was subsequently performed. Pictures were taken with a Zeiss LSM710 confocal microscope and analyzed using ImageJ software. Bars = 2 μm.

(F) *E. coli* bacteria treated for 1 hr with or without 20 μM TAT-RasGAP$_{317-326}$ were fixed with glutaraldehyde and prepared for electron microscopy as described in STAR Methods section. Samples were imaged via transmission electron microscopy. Images were analyzed using ImageJ software. Bars = 2 μm.

TAT-RasGAP$_{317-326}$ alters the transcriptional landscape of *E. coli*

RNA sequencing analysis was performed to evaluate the impact of TAT-RasGAP$_{317-326}$ on *E. coli* transcriptome. For this, we used 10 μM of the peptide, a concentration that prevents *E. coli* proliferation but does not lead to a dramatic drop in bacterial numbers (Figure 2A). Among the 4419 transcripts predicted from the *E. coli* MG1655 genome, 95.6% (n = 4223) were detected in at least one condition (Data S1). Figure 3A presents the fold change in gene expression between bacteria incubated with and without

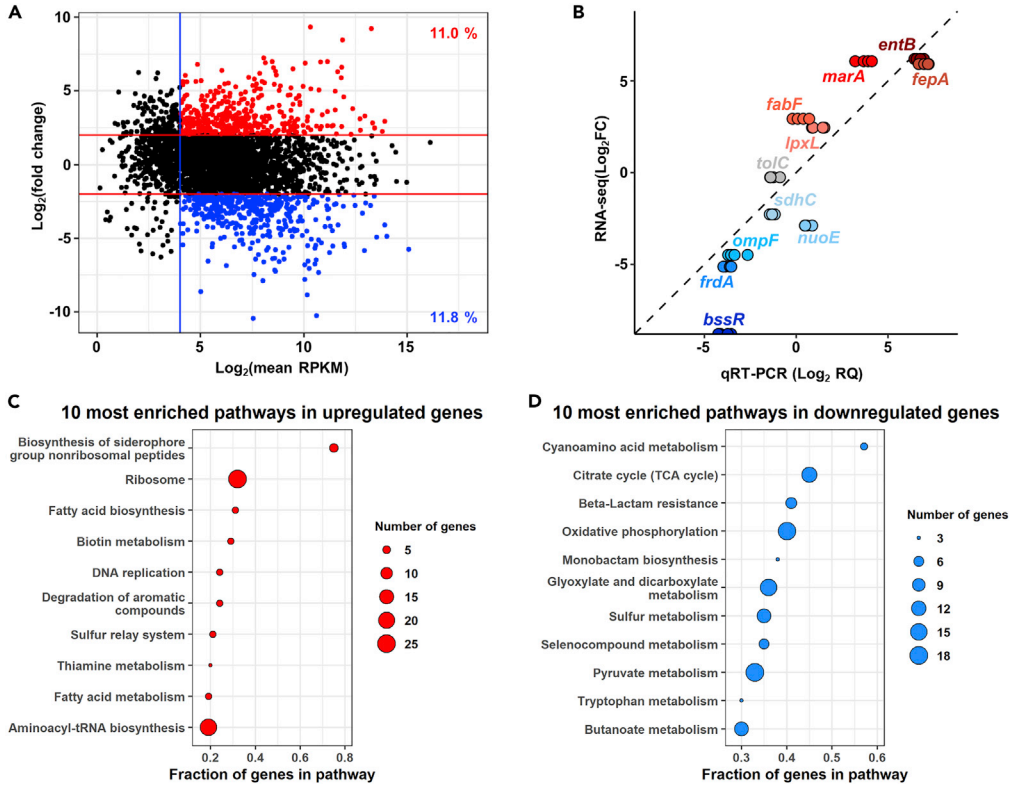

Figure 3. TAT-RasGAP$_{317-326}$ alters the transcriptional landscape of *E. coli*

RNA-seq analysis was performed on *E. coli* MG1655 incubated for 1 hr with or without 10 μM TAT-RasGAP$_{317-326}$.

(A) MA-plot of the average gene expression (x axis, RPKM: read per kilobase million) vs the differential expression (y axis). Threshold for gene expression is indicated with the blue vertical line. The red lines indicate the cut-off limit for upregulated (red dots) and downregulated (blue dots) genes. Detailed results can be found in Data S1 and Tables S1 and S2.

(B) Correlation between RNA-seq (log_2 Fold Change) and qRT-PCR (log_2 Relative Quantification) differential expression performed on RNA extracted from *E. coli* treated for one hour with or without 10 μM TAT-RasGAP$_{317-326}$ for a set of genes detected by RNA-seq as downregulated by the peptide (blue), not changed (gray) or upregulated (red). Gene expression was measured in duplicates on two independent extracted RNA sets.

(C and D) Fraction of KEGG pathway genes that are upregulated (C) or downregulated (D) after treatment with TAT-RasGAP$_{317-326}$. Dot size indicates the number of genes in the selection. See also Figure S5 for GO term analysis.

TAT-RasGAP$_{317-326}$, as well as the average level of expression for each gene. We excluded from our analysis genes whose expression was below the threshold set at 16 reads per kilobase of transcripts per million reads (RPKM). Overall, TAT-RasGAP$_{317-326}$ treatment affected the expression of 962 genes (fold change >4): 11.0% of total detected genes were upregulated (red dots in Figure 3A) while 11.8% were downregulated (blue dots in Figure 3A). Detailed lists of upregulated and downregulated genes can be found in Tables S1 and S2, respectively.

We assessed and validated twelve genes from the RNA-Seq data by qRT-PCR on RNA extracted under the same conditions as for the RNA-Seq analyses. Five of these (*lpxL*, *fabF*, *marA*, *entB*, and *fepA*, depicted in red in Figure 3B) were reported by RNA-Seq as upregulated, five as downregulated (*bssR*, *frdA*, *ompF*, *nuoE*, and *sdhC*, depicted in blue in Figure 3B) and two as unchanged according to the RNA-Seq analysis (*tolC* and *ompR*). One of the unchanged genes, *ompR*, was used as the housekeeping reference gene for normalization. We obtained good correlation between the fold changes obtained with RNA-Seq and with qRT-PCR, confirming the validity of the RNA-Seq data (Figure 3B).

Using the gene expression profiles we obtained from RNA sequencing, we investigated which biological pathways were associated with the *E. coli* response upon exposure to TAT-RasGAP$_{317-326}$. To accomplish this in a systematic manner, we performed Gene Ontology (GO) and Kyoto Encyclopedia of Genes and

Genomes (KEGG) pathway enrichment analyses (Kanehisa and Goto, 2000; Kanehisa et al., 2019; Kanehisa, 2019; Ashburner et al., 2000; The Gene Ontology, 2019) on the subset of differentially expressed genes. The analysis of KEGG pathways revealed that several metabolic and information-processing pathways were enriched among differentially expressed genes (Figures 3C and 3D). For example, seven of the eight genes responsible for enterobactin synthesis in *E. coli* (included in "biosynthesis of siderophore group nonribosomal peptides" KEGG pathway) were upregulated upon peptide treatment. Other metabolic pathways such as carbon metabolism (citrate cycle, pyruvate metabolism) and oxidative phosphorylation were downregulated. Similarly, GO term analysis revealed that upregulated and downregulated genes in response to TAT-RasGAP$_{317-326}$ were enriched in biological processes related to general bacterial metabolism and stress response (Figure S5). From our data, we could not distinguish peptide-specific gene expression changes from gene expression changes mediating general bacterial adaptation to stress. To address this question, we decided to perform a screening of a comprehensive *E. coli* deletion mutant library to determine which genes are directly involved in the bacterial response to TAT-RasGAP$_{317-326}$.

Screening of the Keio *E. coli* deletion mutant library uncovers genes that affect bacterial responses to TAT-RasGAP$_{317-326}$

The Keio collection of *E. coli* deletion mutants consists of single gene deletion clones for each non-essential gene in *E. coli*, in which the gene is replaced by an antibiotic resistance cassette (Baba et al., 2006). To perform the screening of the collection, we exposed each Keio strain to 5 μM TAT-RasGAP$_{317-326}$, a non-bactericidal concentration of peptide (Figure 2A) and monitored bacterial growth by OD_{590} measurement at specific time points (detailed results of growth measurements for all individual mutants are available in Data S2). For each strain, we determined the relative growth of the deletion strain compared to the wild-type strain when incubated with TAT-RasGAP$_{317-326}$ for 6 hr and 24 hr (Figure 4, panels A and B). We identified 27 strains showing decreased sensitivity to the peptide, thus having a normalized growth at 6 hr higher than the average of 270 replicates of the parental strain +2 times the standard deviation (Figure 4A and Table S3). Furthermore, we identified 356 hypersensitive strains (having deletions in 279 different genes) that showed a normalized growth at 24 hr lower than average of the parental strain minus 3 times the standard deviation (Figure 4B). While the wild-type strains grew more slowly in the presence than in the absence of TAT-RasGAP$_{317-326}$, strains showing decreased sensitivity to the peptide grew similarly in both conditions and hypersensitive strains showed no detectable growth in the presence of the peptide (Figure 4C). It has to be mentioned that Keio collection is composed of two independent deletion mutants for each gene. We could not observe decreased sensitivity, as defined by our criteria, in both strains having the same gene deleted (Table S3). However, some decreased sensitivity, approaching the threshold, could be observed in the second strain for a few genes such as *crr* and *rfaY*, for example. The *crr* gene product is involved in glucose uptake and phosphorylation, and in carbon metabolism regulation (Deutscher et al., 2006). The *rfaY* gene product is part of the LPS biogenesis pathway (Yethon et al., 1998). Interestingly, inactivation of *rfaY* by transposon mutagenesis was shown to affect *E. coli* susceptibility to another AMP, LL-37 (Bociek et al., 2015).

On the other hand, 77 gene deletions caused hypersensitivity for both replicates present in the Keio collection (Table S4). KEGG pathway and GO term analyses were thus performed on genes for which both deletion mutants showed hypersensitivity. The results of this analysis indicate that deletion of genes involved in bacterial metabolism and two component systems were associated with TAT-RasGAP$_{317-326}$ bacterial sensitivity (Figures 4D and 4E, Table 2).

Of interest, we found that a subset of less and more sensitive Keio strains were deletion mutants in LPS biogenesis genes. We confirmed differences in sensitivity for *ΔrfaY* and *ΔlpxL* deletion mutants by measuring MIC and IC_{50} of TAT-RasGAP$_{317-326}$ on these mutants and could confirm that deletion of *rfaY* caused a decreased sensitivity and deletion of *lpxL* an increased sensitivity to the peptide (Figure 5A). These mutations had only a limited effect on *E. coli* sensitivity toward the detergent sodium dodecyl-sulfate (Figure S6A), suggesting that these mutations do not affect general membrane integrity. The *rfaY* deletion slightly increased resistance to TAT-RasGAP$_{317-326}$ but had no visible impact on how bacteria responded to polymyxin B and even increased the susceptibility of the bacteria to melittin. Increased resistance conferred by *rfaY* deletion seems therefore to be specific for TAT-RasGAP$_{317-326}$ and not to other membrane disrupting peptides. On the other hand, *lpxL* deletion increased the sensitivity of *E. coli* toward the membrane active peptides melittin and polymyxin B (Figures S6B and S6C). The influence of LPS structure on sensitivity to TAT-RasGAP$_{317-326}$ raises the possibility that TAT-RasGAP$_{317-326}$ directly interacts with bacterial LPS. In such a case, soluble LPS should compete with the peptide for binding to bacterial cells and

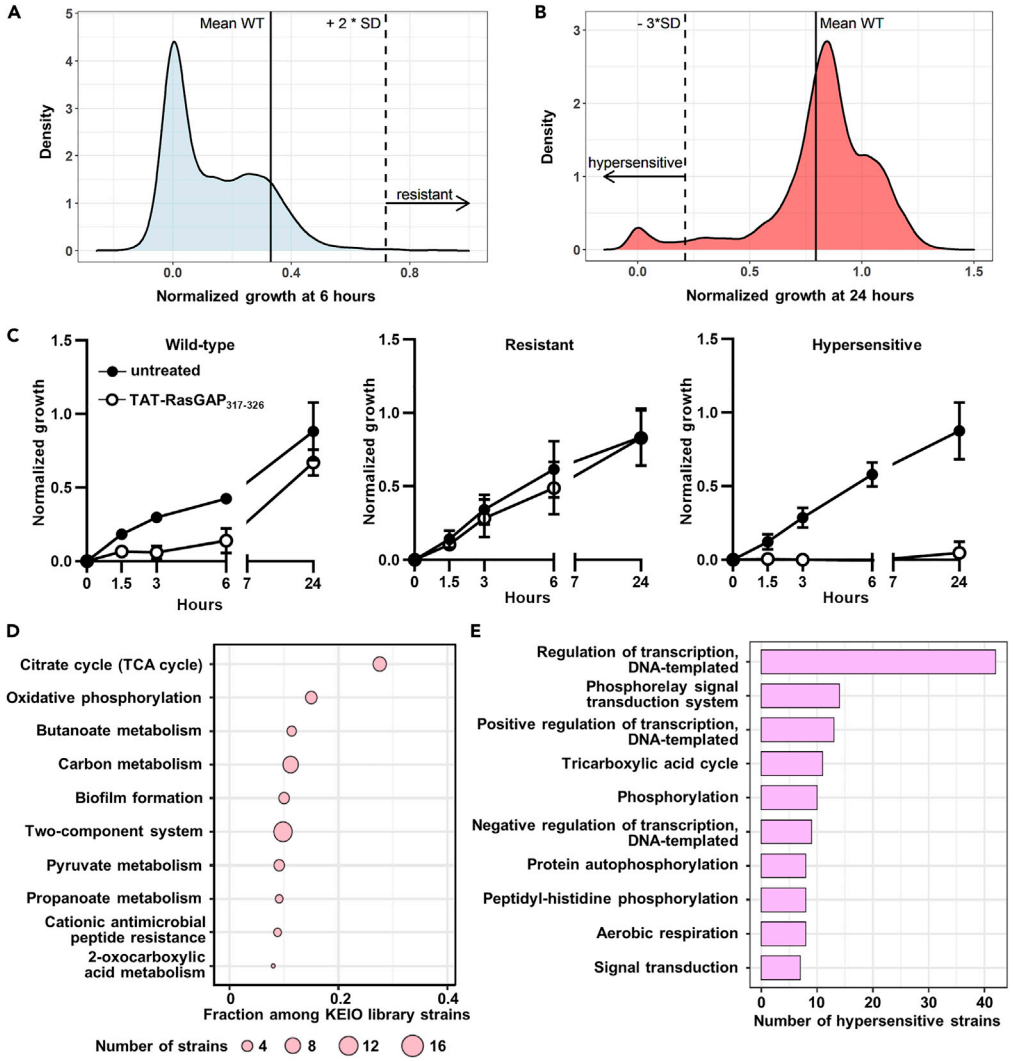

Figure 4. Selection of hypersensitive and resistant *E. coli* deletion mutants from the KEIO collection

Deletion mutants and the corresponding wild-type strain were grown in LB medium with or without 5 μM TAT-RasGAP$_{317-326}$. OD_{590} was measured at 0, 1.5, 3, 6, and 24 hr.

(A and B) Distribution of the normalized growth (NG; see the methods section for its calculation) of bacteria incubated with TAT-RasGAP$_{317-326}$ at 6 hr (A) and 24 hr (B). The mean NG of the wild-type strain (mean WT) is indicated with a vertical solid line. Strains with $NG_{6\ hours}$ > [mean WT + 2 standard deviations (SDs)] and with $NG_{24\ hr}$ < [mean WT - 3 SDs] are defined here as resistant and hypersensitive strains, respectively. Detailed results can be found in Data S2 and Tables S3 and S4.

(C) Growth curves of wild-type (n = 270), hypersensitive (n = 356), and resistant (n = 20) mutants in presence or absence of 5 μM TAT-RasGAP$_{317-326}$. Data are mean ± SD. Error bars are not visible when they are smaller than the symbols.

(D) Top 10 most represented KEGG pathways among hypersensitive strains. The number of hypersensitive strains in each pathway was normalized to the number of KEIO collection strains in the corresponding pathway.

(E) Biological processes GO term enrichment analysis with the 10 most represented terms among the hypersensitive strains.

reduce peptide efficacy, an effect that has been reported for polymyxin B (Domingues et al., 2012). Figure 5B shows indeed that soluble LPS greatly diminishes the efficacy of polymyxin B but has no impact on the sensitivity of *E. coli* toward TAT-RasGAP$_{317-326}$. The potential role played by genes involved in LPS synthesis in TAT-RasGAP$_{317-326}$ sensitivity remains therefore to be uncovered.

We further investigated whether LPS integrity was required for survival of *E. coli* in the presence of TAT-RasGAP$_{317-326}$. For this purpose, we used EDTA to destabilize the LPS structure (Hancock, 1984) and measured

Table 2. List of two-component systems, for which deletion of at least one of the components caused increased sensitivity to TAT-RasGAP$_{317-326}$

Two-component system	Component(s), which deletion cause(s) sensitivity	Conditions regulating the system	Potential link(s) with resistance (Reference)
baeSR	*baeS* (Sensory kinase)	Envelope stress	Overexpression of *baeR* causes resistance to novobiocin and deoxycholate (Baranova and Nikaido, 2002)
citAB	*citB* (DNA binding)	Citrate/anaerobic conditions	
cpxAR	*cpxA* (Sensory kinase)	Inner membrane stress	Upregulates multidrug resistance cascade (Weatherspoon-Griffin et al., 2014)
creCB	**Both**	Carbone source	Hyperactivation causes colicin E2 tolerance (Cariss et al., 2010)
dcuSR	**Both**	Dicarboxylate	
envZ-ompR	**Both**	Medium osmolality	
kdpDE	*kdpD* (Sensory kinase)	Potassium concentration	
phoQP	**Both**	Low magnesium	Involved in resistance to AMPs (Bader et al., 2005)
rcsBC	*rcsC* (Sensory kinase)	Envelope stress	Contributes to intrinsic antibiotic resistance (Laubacher and Ades, 2008)

Data were extracted from the Keio collection screening and genes annotated as two-component system components and showing increased sensitivity for both duplicates were selected. Systems are highlighted in bold when both components were retrieved in the screening. Conditions regulating the systems were extracted from the ecocyc.org database.

how this impacted the MIC of TAT-RasGAP$_{317-326}$ and polymyxin B on two *E. coli* strains lacking (the MG1655 strain) or not (the ATCC 25922 strain) O-antigen moieties (Eder et al., 2009). EDTA, at concentrations that do not affect bacterial proliferation (Figure S7), sensitized both strains to TAT-RasGAP$_{317-326}$ (Figures 5C and 5D), suggesting that compromised LPS integrity favors the antimicrobial activity of the peptide. Polymyxin B sensitivity was less affected by EDTA, indicating again that polymyxin B and TAT-RasGAP$_{317-326}$ might not interact with LPS in identical ways.

Transposon screening in *P. aeruginosa*

Since TAT-RasGAP$_{317-326}$ is active against both *E. coli* and *P. aeruginosa*, we investigated whether some of the pathways that play a role in peptide resistance are shared between the two bacterial species. We thus exposed a *P. aeruginosa* transposon mutant library (Vitale et al., 2020) to 0.5 μM TAT-RasGAP$_{317-326}$ for 12 generations and performed deep sequencing. This allowed us to compare level of transposons in different genes between a bacterial population treated with the peptide and another that was not. Prevalence of strains having a disruption of a gene required for growth in presence of the peptide would decrease compared to strains having integrated the transposon in an unrelated region (detailed results of this deep sequencing are presented as Data S3). We thus defined lower prevalence of transposon insertion as a readout of hypersensitivity to TAT-RasGAP$_{317-326}$. By this way, we identified 75 genes, for which prevalence of disruption via transposon insertion decreased in presence of the peptide (Table S5). Interestingly, 26 of these (35%) are associated with hypersensitivity to other AMPs (Vitale et al., 2020). Some of these genes code for LPS modifying enzymes such as ArnA, ArnB, and ArnT, and for two-component regulators such as ParS and ParR that are involved in the regulation of LPS modifications (Fernandez et al., 2010). Among the genes, for which prevalence of transposon insertion was decreased in presence of TAT-RasGAP$_{317-326}$ but not with other AMPs, we identified *algJ*, *algK*, and *algX*, genes of the biosynthesis pathway of the extracellular polysaccharide alginate. We also observed that mutants in genes coding for the RND efflux transporter MdtABC and CusC, a component of the trans-periplasmic Cu^{2+} transporter CusCFBA, are potentially associated with hypersensitivity to TAT-RasGAP$_{317-326}$. Other pathways that seem to be important for TAT-RasGAP$_{317-326}$ resistance are related to carbon metabolism, redox reactions, and translation regulation (Table S5).

We next compared the lists of potential hypersensitive strains found in screenings in *E. coli* and in *P. aeruginosa*. We identified six gene orthologues, whose disruption is associated with hypersensitivity to the TAT-RasGAP$_{317-326}$ peptide in both *E. coli* and *P. aeruginosa* (Table 3). Among them, four are coding for two-component system proteins: *parR* and *parS* (*rtsA* and *rstB* in *E. coli*), *phoP*, and *pmrB* (*qseC* in

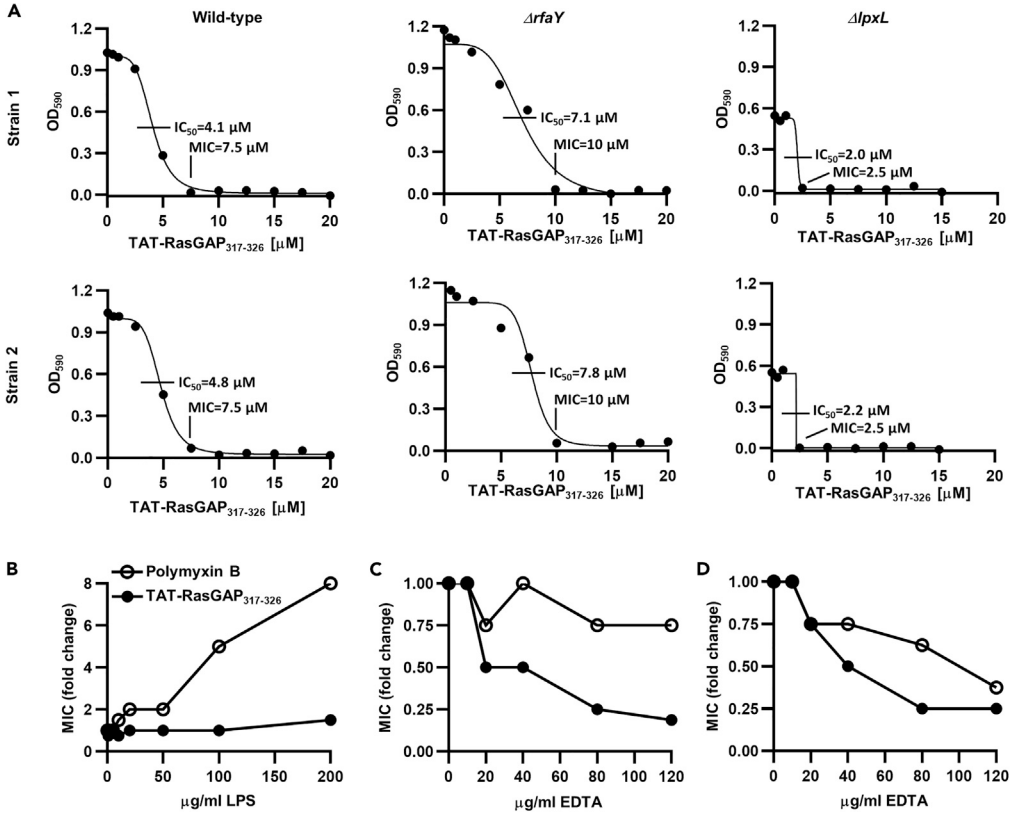

Figure 5. Changes in LPS integrity influence TAT-RasGAP$_{317-326}$ activity

(A) Deletion of LPS biosynthesis genes has diverse effects on TAT-RasGAP$_{317-326}$ activity. MICs and IC_{50} of TAT-RasGAP$_{317-326}$ against wild-type strain or the two deletion mutants *ΔrfaY* resp. *ΔlpxL* from the Keio deletion library were measured as previously described. See also Figure S6 for additional analyses of these mutants.

(B–D) LPS supplementation or EDTA differentially influence activity of TAT-RasGAP$_{317-326}$ and polymyxin (B) MICs of TAT-RasGAP$_{317-326}$ and polymyxin B on *E. coli* MG1655 (A-B) or ATCC25922 (C) were measured as previously described in LB containing the indicated concentrations of purified LPS or EDTA. Data are averages of two independent experiments. See also Figure S7 for additional controls.

E. coli). These four mutants were associated with hypersensitivity to polymyxin B in *P. aeruginosa* (Vitale et al., 2020), indicating that these regulatory pathways may be required for a general adaptation to AMPs. This is of interest, since RstAB system is regulated by PhoPQ system in *E. coli* (Ogasawara et al., 2007) and PhoPQ system was shown to be involved in resistance to AMPs (Yadavalli et al., 2016). Two other genes conserved between *P. aeruginosa* and *E. coli* are associated specifically with hypersensitivity to TAT-RasGAP$_{317-326}$. One is a transcriptional regulator and the other is involved in LPS biosynthesis, further highlighting a potential role for cell surface composition in the sensitivity of bacteria toward TAT-RasGAP$_{317-326}$ (Table 3).

Effect of combining TAT-RasGAP$_{317-326}$ with other AMPs

To determine whether TAT-RasGAP$_{317-326}$ activity is affected by other AMPs, we performed growth tests of *E. coli* in presence of different combinations of TAT-RasGAP$_{317-326}$, melittin, LL-37 and polymyxin B. Concentrations were chosen so that a clear difference in growth was observed when "half" concentrations were used (Figure S8A) as compared with "full" concentrations that correspond to the double of "half" concentrations (Figure S8B). The effect of combining pairs of AMPs using "half" concentrations is shown in Figure S8C as percentage of growth compared with an untreated control. We did not observe an increase in the effect of TAT-RasGAP$_{317-326}$ when combined with the three other AMPs. However, the combination of melittin and polymyxin B (2.7% of growth) and the combination of LL-37 and polymyxin B (0.6% of growth) showed increased activity. Notably, the combination of melittin and polymyxin B caused stronger growth inhibition (>95%) than obtained by either compound at the "full" concentration (~20% and ~35% growth

Table 3. Genes found as more sensitive in both *P. aeruginosa* by transposon library screening and in *E. coli* by Keio collection screening

Locus_tag	Gene_ symbol	Description	Category	Log_2(FC_ BM2vsTATRasGAP)	Hypersensitivity to polymyxin B	*E. coli* homologs
PA14_41,260	*parR*	Two-component response regulator	Two-component regulator system	−4.268533546	Yes	*rstA*
PA14_41,270	*parS*	Two-component sensor	Two-component regulator system	NA	Yes	*rstB*
PA14_49,180	*phoP*	Two-component response regulator	Two-component regulator system	NA	Yes	*phoP*
PA14_63,160	*pmrB*	Two-component regulator system signal sensor kinase	Two-component regulator system	−3.492272393	Yes	*qseC*
PA14_02,390		Transcriptional regulator	Transcription regulation	−5.436478184		*cynR*
PA14_71,970	*wbpW*	GDP-mannose pyrophosphorylase	LPS biosynthesis	−4.335647742		*cpsB*

List of the genes, whose disruption generated mutant strains found as sensitive in transposon library screening in *P. aeruginosa* and whose orthologues in *E. coli* were detected as sensitive in Keio collection screening. Transposon mutants of *P. aeruginosa* were incubated in presence or absence of 0.5 μM TAT-$RasGAP_{317-326}$ in BM2 Mg^{low} medium for 12 generations. Transposon junctions were amplified and sequenced. Fold change (FC) between abundance of transposon mutants with incubation in absence (BM2) or presence (TATRasGAP) of the peptide was calculated and values are presented as Log_2 of the FC. NA indicates that no mutant was detected upon peptide treatment, and therefore Log_2 of the FC could not be calculated. Complete results can be found in Data S3 and Table S5. Shown also are results obtained in a former study using the same transposon library that indicate which gene disruptions also cause hypersensitivity to polymyxin B (Vitale et al., 2020).

inhibition for melittin and polymyxin B, respectively; Figure S8C). This observation is consistent with previous reports of the synergism between melittin and antibiotics such as doripenem and ceftazidime (Akbari et al., 2019). In contrast, we observed an apparent lower effect of TAT-$RasGAP_{317-326}$ in presence of melittin (Figure S8C). Since this effect was very weak in these conditions, we combined the "half" concentration of melittin with the "full" concentration of TAT-$RasGAP_{317-326}$ and could observe a clear inhibition of the antimicrobial activity of this peptide by melittin (Figure 6A). To better understand the mechanism behind this observation, we assessed peptide binding and entry into bacteria using a fluorescently labeled version of TAT-$RasGAP_{317-326}$ peptide. We found that, in the presence of melittin, binding of FITC-labeled TAT-$RasGAP_{317-326}$ to *E. coli* bacteria was not decreased but apparently slightly increased when compared with the control condition where bacteria were incubated with FITC-labeled TAT-$RasGAP_{317-326}$ alone. However, we observed an apparent lower intracellular accumulation of the labeled version of TAT-$RasGAP_{317-326}$ peptide in presence of melittin (Figure 6B).

In vitro selection of resistant bacteria to TAT-$RasGAP_{317-326}$ peptide

AMPs are less susceptible to bacterial resistance evolution than classical antibiotics (Lazar et al., 2018; Spohn et al., 2019; Lazzaro et al., 2020). To measure the propensity of bacteria to develop resistance against TAT-$RasGAP_{317-326}$, we serially passaged several bacterial strains (*E. coli*, *P. aeruginosa*, *S. aureus* and *S. capitis*) in the presence of TAT-$RasGAP_{317-326}$ peptide and recorded the number of passages required to detect the appearance of resistant mutants in each strain. First, we grew the parental bacterial strains overnight in presence of sub-inhibitory concentrations of the peptide. We then diluted this parent culture into two subcultures, one of which was exposed to an increased concentration of the TAT-$RasGAP_{317-326}$ peptide while the other was kept in the same concentration of peptide as the parent culture. Once bacterial growth was detected in the culture exposed to an elevated concentration of the peptide, the process was repeated, thereby exposing the bacterial culture to sequentially increasing concentrations of peptide for a total of 20 passages. For each passage, we measured the corresponding MIC (Figure 7A). Using this approach, we obtained strains with highly increased MICs (16–32 fold) for *E. coli*, *S. capitis* but only a small increase (2–4 fold) for *P. aeruginosa* (Figure 7A, Table 4 and Tables S6–S8). It should be noted that the parental strain of *S. aureus* has a peptide MIC in the range of 64–128 μM and this MIC rapidly increased to 256 μM (Table S9). We did not expose bacteria to higher concentrations, as the peptide started to precipitate in these conditions. To test whether the strains recovered at passage 20 for *E. coli*, *P. aeruginosa*, and *S. capitis* and passage 12 for *S. aureus* showed increased resistance to other AMPs as well, we

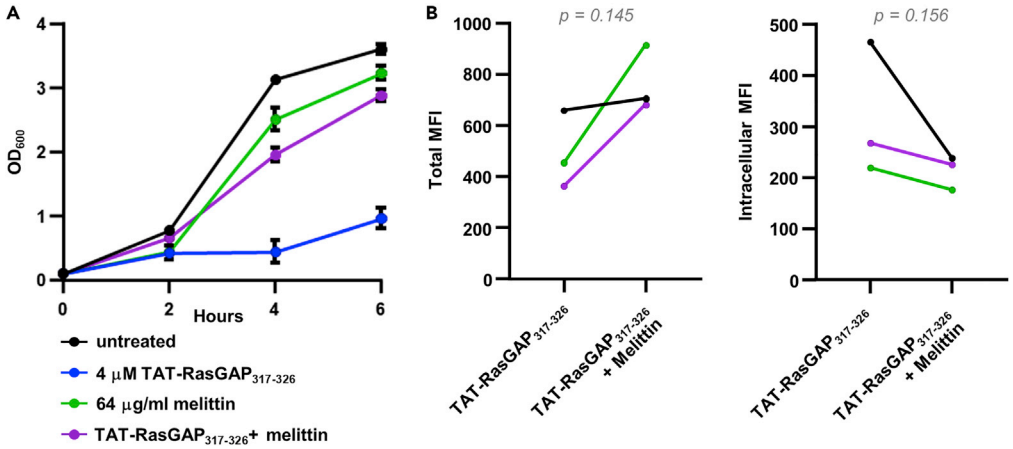

Figure 6. Melittin has an inhibitory effect on TAT-RasGAP$_{317-326}$ activity

(A) Sub-inhibitory concentrations of melittin interfere with TAT-RasGAP$_{317-326}$ activity. Indicated concentrations of AMPs were added and OD_{600} was measured as previously described. Average and range of two independent experiments are shown.

(B) *E. coli* MG1655 was grown overnight at 37°C, diluted to OD_{600} = 0.1, and grown during 1 hr before addition or not of 10 μM FITC-labeled TAT-RasGAP$_{317-326}$ with or without 64 μg/mL melittin. Cells were incubated for 1 hr at 37°C, extracellular fluorescence was quenched (Intracellular) or not (Total) using 0.2% trypan blue before sample acquisition. Mean fluorescence intensities (MFI) were measured for triplicates (shown with different colors). p values were calculated using ratio paired t test between the indicated conditions. Detailed results of all AMPs combinations tested can be found in Figure S8.

determined the fold change of the MICs for polymyxin B, melittin and LL-37 relative to the corresponding parental strains that did not undergo selection (Table 4). Interestingly, peptide-resistant *E. coli* (Gram-negative) did not show increased MICs to the other AMPs we tested as compared to the parental strain. In contrast, *P. aeruginosa* and the Gram-positive *S. aureus* and *S. capitis* selected for resistance to TAT-RasGAP$_{317-326}$ showed increased MIC toward other AMPs (Table 4). Thus, our findings suggest that bacterial species differ in their tendency to develop cross-resistance to TAT-RasGAP$_{317-326}$ peptide and other AMPs.

Finally, we sought to investigate whether the peptide-resistant bacteria we obtained in our selection process remain targets for alternative treatments such as combination therapy with other antimicrobial agents. In particular, we tested whether EDTA, an agent known to enhance the efficacy of antimicrobials via a mechanism that weakens the outer cell wall of bacteria, could potentiate the effect of TAT-RasGAP$_{317-326}$ against peptide-resistant *E. coli* (Leive, 1965). Importantly, the presence of EDTA alone at the concentrations tested was not associated with any significant change in bacterial numbers (Figure S7). However, EDTA in combination with TAT-RasGAP$_{317-326}$ (Figure 7B) potentiated the ability of the peptide against the peptide-resistant *E. coli* strain. Our findings suggest that peptide-resistance remains treatable in combination therapy with other antimicrobial agents.

DISCUSSION

The activity of AMPs can be affected by environmental factors, but we lack knowledge about how extracellular factors impact TAT-RasGAP$_{317-326}$ activity. Here, we report that addition of divalent cations in LB medium resulted in decreased bacterial sensitivity to TAT-RasGAP$_{317-326}$ peptide and reduced peptide binding and entry. The mechanism contributing to lower peptide binding might be due to competition between divalent ions in the culture medium and the cationic TAT-RasGAP$_{317-326}$ peptide for binding to bacterial surface (Figure 8). Alternatively, divalent cations, which are important for membrane stability, may influence binding and entry of TAT-RasGAP$_{317-326}$ (Clifton et al., 2015). The strong dependence of TAT-RasGAP$_{317-326}$ to medium composition is of interest. In rich media, the MIC of this peptide toward *P. aeruginosa* is 32 μM, while, in synthetic medium such as BM2 Mg^{low}, the MIC of TAT-RasGAP$_{317-326}$ is 4 μM.

RNA sequencing showed that genes involved in carbon metabolism were downregulated upon treatment with TAT-RasGAP$_{317-326}$ (Figure 3). Moreover, deletion or transposon mutants of genes involved in carbon metabolism and ATP production were more sensitive toward TAT-RasGAP$_{317-326}$ (Figure 4 and Table 3),

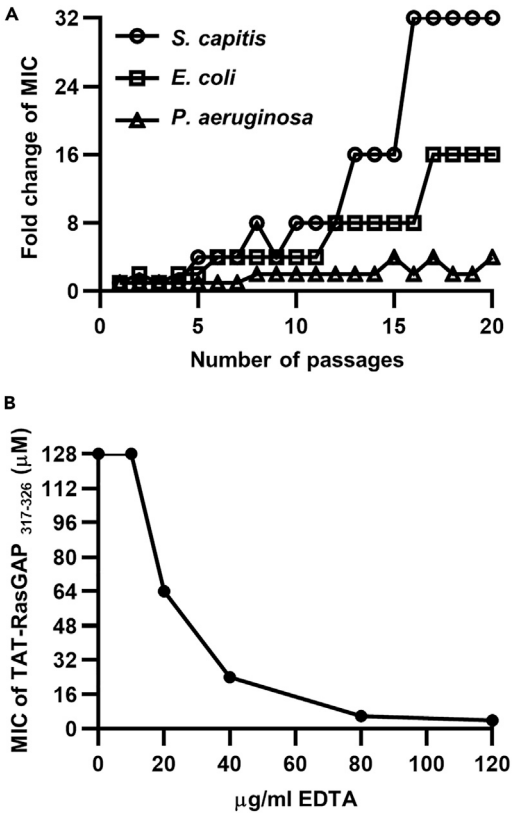

Figure 7. Bacterial resistance against TAT-RasGAP$_{317-326}$ appears after selection with sub-inhibitory concentrations of peptide

(A) The indicated strains were incubated in presence or absence of 0.5 MIC of TAT-RasGAP$_{317-326}$. Cultures were then diluted each day in medium containing either the same concentration of the peptide or an increased concentration. Once bacterial growth was detected in the culture exposed to an elevated concentration of the peptide, the process was repeated thereby exposing the bacterial culture to sequentially increasing concentrations of peptide for a total of 20 passages. MIC of each passage was then measured and is presented as a fold change compared with the MIC of the original strain passaged in the absence of peptide.

(B) Peptide-resistant *E. coli* is susceptible to peptide activity during combination treatment with EDTA. MIC of *E. coli* strain selected for 20 passages from (A) was measured in presence of increasing concentrations of EDTA. Average of two independent experiments is presented.

indicating that energy production pathways may be important for resistance toward this peptide. Adaptation to environmental stimuli might also be of importance for survival to TAT-RasGAP$_{317-326}$, since mutants lacking genes coding for some two-component systems show increased sensitivity toward TAT-RasGAP$_{317-326}$ (Table 2). Several of these two-component systems are known to play roles in resistance to antibiotics or AMPs, such as PhoPQ, whose importance in response to AMPs is well described (Bader et al., 2005; Yadavalli et al., 2016). This further highlights the importance of two-component systems for adaptability and survival of bacteria in harsh conditions.

Another pathway that may be involved in sensitivity to TAT-RasGAP$_{317-326}$ is the LPS biosynthesis pathway. We found that some mutations affecting this pathway cause either moderate resistance or hypersensitivity to the peptide. Indeed, deletion of *rfaY*, coding for a LPS kinase, caused a slight increase of the MIC of TAT-RasGAP$_{317-326}$, but had no influence on the MIC of melittin and polymyxin B (Figures 5A and S6) (Yethon et al., 1998). In contrast, deletion of *lpxL*, coding for a lauroyl acyltransferase that is required for synthesis of the precursor of LPS lipid A induced hypersensitivity to several AMPs (Six et al., 2008) (Figures 5A and S6). Interestingly, LPS modifications in our LPS mutants differentially affect the activities of TAT-RasGAP$_{317-326}$ and polymyxin B, potentially as a result of differences in interaction of these peptides with bacterial surfaces. We could further confirm the importance of LPS integrity for survival to TAT-RasGAP$_{317-326}$ using EDTA that destabilizes LPS. This is consistent with the protective effect of divalent cations (Figure 1), which

Table 4. MICs of TAT-RasGAP$_{317-326}$-resistant strains toward other AMPs

	TAT-RasGAP$_{317-326}$	Polymyxin B	Melittin	LL-37
E. coli	16	0.5	0.5	0.5
P. aeruginosa	4	2	>2	ND
S. capitis	32	>2	2	ND
S. aureus	>2	ND	8	ND

Fold change of MICs between the original strains (*E. coli* MG1655, *P. aeruginosa* PA14, *S. capitis*, and *S. aureus* ATCC 29213) and strains exposed to increasing concentrations of TAT-RasGAP$_{317-326}$ for 20 passages. MICs were measured as described for Figure 1. ND: MIC of the strain could not be determined. Detailed results are presented in Tables S6–S9.

can bind and stabilize LPS (Pelletier et al., 1994). Importance of bacterial surface composition in sensitivity toward TAT-RasGAP$_{317-326}$ is further highlighted by the fact that *P. aeruginosa* transposon mutants affecting the alginate biosynthesis pathway are more sensitive to TAT-RasGAP$_{317-326}$ than the control strain (Table S5). Alginate is an anionic extracellular polysaccharide that is involved in virulence, antimicrobial resistance and biofilm formation in *P. aeruginosa* (Franklin et al., 2011).

Screening of the Keio deletion collection did not allow to unearth mutants showing complete resistance toward TAT-RasGAP$_{317-326}$. This indicates that resistance may not be obtained by the loss of function of one gene. Resistant strains toward TAT-RasGAP$_{317-326}$ that we obtained by selection (Figure 7A) may thus have acquired point mutations that modulate activity through activation of some pathways or modifications of essential components. This needs now further investigations in order to describe mechanisms of resistance toward TAT-RasGAP$_{317-326}$ in particular and AMPs in general.

On the other hand, Keio collection screening highlighted pathways that are apparently required for *E. coli* to respond to TAT-RasGAP$_{317-326}$. Whether these pathways are specifically required for response to TAT-RasGAP$_{317-326}$ or play a role in a general response to AMPs needs further investigation. Interestingly, we observed, using a *P. aeruginosa* transposon mutants library, that 21% (16 out of 75) of the genes which mutation was association with hypersensitivity to TAT-RasGAP$_{317-326}$ were associated with hypersensitivity toward other AMPs (Table S5) (Vitale et al., 2020).

Combinatorial therapies are gaining interest in the treatment of multi-resistant bacteria (Leon-Buitimea et al., 2020). We thus investigated whether combination with other AMPs might influence the activity of TAT-RasGAP$_{317-326}$. In general, activity of TAT-RasGAP$_{317-326}$ was not influenced by other AMPs. However, melittin had an inhibitory effect on TAT-RasGAP$_{317-326}$ activity, affecting its entry in bacteria (Figure 6). This rather peculiar effect might be explained by the hypothesized mode of action of melittin (i.e. carpet model), in which melittin first interacts with the bacterial surface, before reaching a concentration threshold that leads to the disruption of the bacterial membrane (Lee et al., 2013). Sub-inhibitory concentrations of melittin might thus block binding of TAT-RasGAP$_{317-326}$ to the bacterial membrane.

Finally, we investigated the potency of bacteria to develop resistance toward TAT-RasGAP$_{317-326}$. Resistance could be obtained upon passages in sub-inhibitory concentrations of the peptide (Figure 7A), but bacterial strains differed with respect to the rate of resistance emergence. Interestingly, peptide-resistant *E. coli* remains treatable by peptide in combination with EDTA, a chemical agent that compromises the integrity of the bacterial outer membrane. Future work should examine the mechanism of *E. coli* resistance to peptide and will help elucidate how EDTA, which targets the bacterial envelope, helps potentiate peptide activity in resistant backgrounds. Overall, our data highlight the potential benefit of combination therapies, which might not only prevent the development of such resistance, but also potentiate treatment of resistant strains, as shown here by EDTA in combination with TAT-RasGAP$_{317-326}$.

The schemes presented in Figure 8 highlight the factors that may influence TAT-RasGAP$_{317-326}$ activity and present hypotheses about underlying mechanisms. The positively charged TAT-RasGAP$_{317-326}$ peptide interacts with the negative surface charges of the bacterial membrane, allowing its binding and entry in the bacterial cell (Figure 8A). Presence of divalent cations in the culture medium competes with TAT-RasGAP$_{317-326}$ peptide for binding to the negative charges on LPS, lowering the activity of the peptide. Similarly, modifications of LPS structure can also lower interaction between TAT-RasGAP$_{317-326}$ and bacterial surface. We hypothesize this lower activity to be due to a decrease of the net charge of bacterial surface,

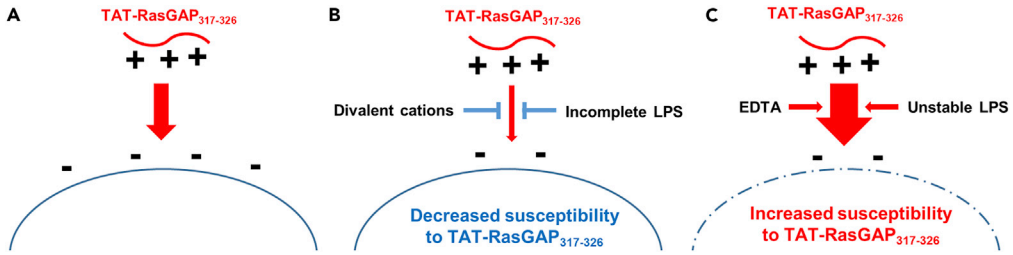

Figure 8. Hypothetical model of the influence of Gram-negative bacterial cell surface modifications on TAT-RasGAP$_{317-326}$ efficiency

(A) Positively charged TAT-RasGAP$_{317-326}$ has affinity for the negatively charged bacterial surface (mostly attributed to the negatively charged LPS structures). Peptide is active (red arrow) and can exert its antibacterial effects.

(B) Conditions that lower the affinity of TAT-RasGAP$_{317-326}$ to the Gram-negative bacterial surface. Divalent cations which possess positive charges compete with TAT-RasGAP$_{317-326}$ for the negatively charged bacterial surface. Similarly, genetic mutations in LPS biosynthesis pathway that reduce the net negative charge of LPS can result in bacterial mutants with reduced peptide binding. In these circumstances, susceptibility of bacteria to TAT-RasGAP$_{317-326}$ is reduced (indicated by a narrow red arrow).

(C) Conditions that increase the effect of TAT-RasGAP$_{317-326}$ toward Gram-negative bacteria. Chemicals that target the bacterial outer membrane, such as EDTA and bacterial mutants with defects in LPS biosynthesis that result in a compromised outer membrane structure are associated with increased susceptibility to TAT-RasGAP$_{317-326}$ (indicated by a broad red arrow).

causing a lower affinity of the peptide to bacteria (Figure 8B). In contrast, destabilization of LPS by EDTA or by deletion of genes involved in biosynthesis of LPS precursors increases the bactericidal activity of TAT-RasGAP$_{317-326}$. This is possibly due to a defect of the integrity of the bacterial envelope, decreasing bacterial defenses toward TAT-RasGAP$_{317-326}$. (Figure 8C).

In summary, the results presented in this article bring a better understanding of the factors that influence the antimicrobial activity of TAT-RasGAP$_{317-326}$. We describe the importance of bacterial envelope integrity on the sensitivity toward TAT-RasGAP$_{317-326}$. Factors such as divalent salts, EDTA and LPS structure influence the concentration of peptide needed to inhibit bacterial growth. Furthermore, we report the effect of TAT-RasGAP$_{317-326}$ on the transcriptional landscape of *E. coli* and highlight the importance of a broad range of two-component systems in the adaptation of bacteria toward this AMP. We finally investigated the effect of other AMPs on the activity of TAT-RasGAP$_{317-326}$ and could select TAT-RasGAP$_{317-326}$-resistant bacteria. Our observation that sensitivity could be increased and resistance could be reversed by addition of EDTA is important in the perspective of a clinical use of this peptide to improve its efficiency and to prevent rapid emergence of resistance.

Limitations of the study

Results presented in this study originate from *in vitro* studies and might not be fully representative of *in vivo* circumstances. For example, how TAT-RasGAP$_{317-326}$ may interact with other exogenous or endogenous AMPs *in vivo*, as well as serum proteins and components remains to be investigated. Moreover, interactions between TAT-RasGAP$_{317-326}$ and other AMPs should be studied in more detail in future assays such as checkerboard assays, in order to determine putative synergisms. Similarly, mechanisms of action of the peptide and mechanisms of resistance toward the peptide will be studied by our lab in the future, in order to describe how TAT-RasGAP$_{317-326}$ interacts with bacteria at the molecular level. Even though the peptide displays minimal toxicity to normal (i.e. non tumoral) mammalian cells (Pittet et al., 2007; Michod et al., 2009; Tsoutsou et al., 2017; Heulot et al., 2016), one may want to modify it such as to decrease even more its toxicity toward mammalian cells but keeping, or even increasing, its activity toward bacteria.

STAR★METHODS

Detailed methods are provided in the online version of this paper and include the following:

- KEY RESOURCES TABLE
- RESOURCE AVAILABILITY
  - Lead contact

SUPPLEMENTAL INFORMATION

Supplemental information can be found online at https://doi.org/10.1016/j.isci.2021.102923.

ACKNOWLEDGMENTS

We would like to thank Sébastien Aeby and Yasmina Merzouk for technical support, Jean Daraspe from the Electron Microscopy Facility of the University of Lausanne for support with electron microscopy, Valentin Scherz for support in bioinformatics analyses, and Prof. Gilbert Greub for sharing equipment and laboratories. This study was supported by an interdisciplinary grant of the Faculty of Biology and Medicine of the University of Lausanne.

AUTHOR CONTRIBUTIONS

M.G., T.H., N.J., A.V., S.H. and S.C. performed experiments. M.G., T.H., L.E., C.W., and N.J. were involved in the planning of the project and discussed the results. M.G., T.H., N.J. and T.P. analyzed the results. M.G., C.W. and N.J. wrote the manuscript. All the authors proofread the manuscript.

DECLARATION OF INTERESTS

The authors declare no competing interests.

Received: May 5, 2021
Revised: July 5, 2021
Accepted: July 27, 2021
Published: August 20, 2021

REFERENCES

Akbari, R., Hakemi-Vala, M., Pashaie, F., Bevalian, P., Hashemi, A., and Pooshang Bagheri, K. (2019). Highly synergistic effects of melittin with conventional antibiotics against multidrug-resistant isolates of acinetobacter baumannii and Pseudomonas aeruginosa. Microb. Drug Resist. *25*, 193–202.

Anders, S., Pyl, P.T., and Huber, W. (2015). HTSeq–a Python framework to work with high-throughput sequencing data. Bioinformatics *31*, 166–169.

Annibaldi, A., Heulot, M., Martinou, J.C., and Widmann, C. (2014). TAT-RasGAP317-326-mediated tumor cell death sensitization can occur independently of Bax and Bak. Apoptosis *19*, 719–733.

Ashburner, M., Ball, C.A., Blake, J.A., Botstein, D., Butler, H., Cherry, J.M., Davis, A.P., Dolinski, K., Dwight, S.S., Eppig, J.T., et al. (2000). Gene ontology: tool for the unification of biology. The Gene Ontology Consortium. Nat. Genet. *25*, 25–29.

Baba, T., Ara, T., Hasegawa, M., Takai, Y., Okumura, Y., Baba, M., Datsenko, K.A., Tomita, M., Wanner, B.L., and Mori, H. (2006). Construction of Escherichia coli K-12 in-frame, single-gene knockout mutants: the Keio collection. Mol. Syst. Biol. *2*, 2006 0008.

Bader, M.W., Sanowar, S., Daley, M.E., Schneider, A.R., Cho, U., Xu, W., Klevit, R.E., Le Moual, H., and Miller, S.I. (2005). Recognition of antimicrobial peptides by a bacterial sensor kinase. Cell *122*, 461–472.

Baranova, N., and Nikaido, H. (2002). The baeSR two-component regulatory system activates transcription of the yegMNOB (mdtABCD) transporter gene cluster in Escherichia coli and increases its resistance to novobiocin and deoxycholate. J. Bacteriol. *184*, 4168–4176.

Barras, D., Chevalier, N., Zoete, V., Dempsey, R., Lapouge, K., Olayioye, M.A., Michielin, O., and Widmann, C. (2014a). A WXW motif is required for the anticancer activity of the TAT-RasGAP317-326 peptide. J. Biol. Chem. *289*, 23701–23711.

Barras, D., Lorusso, G., Lhermitte, B., Viertl, D., Ruegg, C., and Widmann, C. (2014b). Fragment N2, a caspase-3-generated RasGAP fragment, inhibits breast cancer metastatic progression. Int. J. Cancer *135*, 242–247.

Barras, D., Lorusso, G., Ruegg, C., and Widmann, C. (2014c). Inhibition of cell migration and invasion mediated by the TAT-RasGAP317-326 peptide requires the DLC1 tumor suppressor. Oncogene *33*, 5163–5172.

Bociek, K., Ferluga, S., Mardirossian, M., Benincasa, M., Tossi, A., Gennaro, R., and Scocchi, M. (2015). Lipopolysaccharide phosphorylation by the WaaY kinase affects the susceptibility of Escherichia coli to the human antimicrobial peptide LL-37. J. Biol. Chem. *290*, 19933–19941.

Bolger, A.M., Lohse, M., and Usadel, B. (2014). Trimmomatic: a flexible trimmer for Illumina sequence data. Bioinformatics *30*, 2114–2120.

Brogden, K.A. (2005). Antimicrobial peptides: pore formers or metabolic inhibitors in bacteria? Nat. Rev. Microbiol. *3*, 238–250.

Cariss, S.J., Constantinidou, C., Patel, M.D., Takebayashi, Y., Hobman, J.L., Penn, C.W., and Avison, M.B. (2010). YieJ (CbrC) mediates CreBC-dependent colicin E2 tolerance in Escherichia coli. J. Bacteriol. *192*, 3329–3336.

Carslon, M. (2019). GO.db: A Set of Annotation Maps Describing the Entire Gene Ontology. https://doi.org/10.18129/B9.bioc.GO.db.

Clifton, L.A., Skoda, M.W., Le Brun, A.P., Ciesielski, F., Kuzmenko, I., Holt, S.A., and Lakey, J.H. (2015). Effect of divalent cation removal on the structure of gram-negative bacterial outer membrane models. Langmuir *31*, 404–412.

Deutscher, J., Francke, C., and Postma, P.W. (2006). How phosphotransferase system-related protein phosphorylation regulates carbohydrate metabolism in bacteria. Microbiol. Mol. Biol. Rev. *70*, 939–1031.

Di Somma, A., Moretta, A., Cane, C., Cirillo, A., and Duilio, A. (2020). Antimicrobial and antibiofilm peptides. Biomolecules *10*, 652.

Domingues, M.M., Inacio, R.G., Raimundo, J.M., Martins, M., Castanho, M.A., and Santos, N.C. (2012). Biophysical characterization of polymyxin B interaction with LPS aggregates and membrane model systems. Biopolymers *98*, 338–344.

Eder, K., Vizler, C., Kusz, E., Karcagi, I., Glavinas, H., Balogh, G.E., Vigh, L., Duda, E., and Gyorfy, Z. (2009). The role of lipopolysaccharide moieties in macrophage response to Escherichia coli. Biochem. Biophys. Res. Commun. *389*, 46–51.

Fernandez, L., Gooderham, W.J., Bains, M., McPhee, J.B., Wiegand, I., and Hancock, R.E. (2010). Adaptive resistance to the "last hope" antibiotics polymyxin B and colistin in Pseudomonas aeruginosa is mediated by the novel two-component regulatory system ParR-ParS. Antimicrob. Agents Chemother. *54*, 3372–3382.

Fernandez, L., Jenssen, H., Bains, M., Wiegand, I., Gooderham, W.J., and Hancock, R.E. (2012). The two-component system CprRS senses cationic peptides and triggers adaptive resistance in Pseudomonas aeruginosa independently of ParRS. Antimicrob. Agents Chemother. *56*, 6212–6222.

Franklin, M.J., Nivens, D.E., Weadge, J.T., and Howell, P.L. (2011). Biosynthesis of the Pseudomonas aeruginosa extracellular polysaccharides, alginate, Pel, and Psl. Front. Microbiol. *2*, 167.

Gallagher, L.A., Ramage, E., Patrapuvich, R., Weiss, E., Brittnacher, M., and Manoil, C. (2013). Sequence-defined transposon mutant library of Burkholderia thailandensis. mBio *4*, e00604–e00613.

Gallagher, L.A., Shendure, J., and Manoil, C. (2011). Genome-scale identification of resistance functions in Pseudomonas aeruginosa using Tn-seq. mBio *2*, e00315–10.

Gennaro, R., Skerlavaj, B., and Romeo, D. (1989). Purification, composition, and activity of two bactenecins, antibacterial peptides of bovine neutrophils. Infect. Immun. *57*, 3142–3146.

Hancock, R.E. (1997). The bacterial outer membrane as a drug barrier. Trends Microbiol. *5*, 37–42.

Hancock, R.E.W. (1984). Alterations in outer-membrane permeability. Annu. Rev. Microbiol. *38*, 237–264.

Hassan, M., Kjos, M., Nes, I.F., Diep, D.B., and Lotfipour, F. (2012). Natural antimicrobial peptides from bacteria: characteristics and potential applications to fight against antibiotic resistance. J. Appl. Microbiol. *113*, 723–736.

Heinonen, T., Hargraves, S., Georgieva, M., Widmann, C., and Jacquier, N. (2021). The antimicrobial peptide TAT-RasGAP$_{317-326}$ inhibits the formation and the expansion of bacterial biofilms in vitro. J. Glob. Antimicrob. Resist *25*, 227–231.

Heulot, M., Chevalier, N., Puyal, J., Margue, C., Michel, S., Kreis, S., Kulms, D., Barras, D., Nahimana, A., and Widmann, C. (2016). The TAT-RasGAP317-326 anti-cancer peptide can kill in a caspase-, apoptosis-, and necroptosis-independent manner. Oncotarget *7*, 64342–64359.

Heulot, M., Jacquier, N., Aeby, S., Le Roy, D., Roger, T., Trofimenko, E., Barras, D., Greub, G., and Widmann, C. (2017). The anticancer peptide TAT-RasGAP317-326 exerts broad antimicrobial activity. Front. Microbiol. *8*, 994.

Higgins, S., Sanchez-Contreras, M., Gualdi, S., Pinto-Carbo, M., Carlier, A., and Eberl, L. (2017). The essential genome of Burkholderia cenocepacia H111. J. Bacteriol. *199*, e00260-17.

Hong, J., Lu, X., Deng, Z., Xiao, S., Yuan, B., and Yang, K. (2019). How melittin inserts into cell membrane: conformational changes, inter-peptide cooperation, and disturbance on the membrane. Molecules *24*, 1775.

Jevprasesphant, R., Penny, J., Attwood, D., and D'Emanuele, A. (2004). Transport of dendrimer nanocarriers through epithelial cells via the transcellular route. J. Control. Release *97*, 259–267.

Kanehisa, M. (2019). Toward understanding the origin and evolution of cellular organisms. Protein Sci. *28*, 1947–1951.

Kanehisa, M., and Goto, S. (2000). KEGG: kyoto encyclopedia of genes and genomes. Nucleic Acids Res. *28*, 27–30.

Kanehisa, M., Sato, Y., Furumichi, M., Morishima, K., and Tanabe, M. (2019). New approach for understanding genome variations in KEGG. Nucleic Acids Res. *47*, D590–D595.

Kong, X.D., Moriya, J., Carle, V., Pojer, F., Abriata, L.A., Deyle, K., and Heinis, C. (2020). De novo development of proteolytically resistant therapeutic peptides for oral administration. Nat. Biomed. Eng. *4*, 560–571.

Kremer, J.R., Mastronarde, D.N., and McIntosh, J.R. (1996). Computer visualization of three-dimensional image data using IMOD. J. Struct. Biol. *116*, 71–76.

Kumar, P., Kizhakkedathu, J.N., and Straus, S.K. (2018). Antimicrobial peptides: diversity, mechanism of action and strategies to improve the activity and biocompatibility in vivo. Biomolecules *8*, 4.

Laubacher, M.E., and Ades, S.E. (2008). The Rcs phosphorelay is a cell envelope stress response activated by peptidoglycan stress and contributes to intrinsic antibiotic resistance. J. Bacteriol. *190*, 2065–2074.

Lazar, V., Martins, A., Spohn, R., Daruka, L., Grezal, G., Fekete, G., Szamel, M., Jangir, P.K., Kintses, B., Csorgo, B., et al. (2018). Antibiotic-resistant bacteria show widespread collateral sensitivity to antimicrobial peptides. Nat. Microbiol. *3*, 718–731.

Lazzaro, B.P., Zasloff, M., and Rolff, J. (2020). Antimicrobial peptides: Application informed by evolution. Science *368*, eaau5480.

Lee, M.T., Sun, T.L., Hung, W.C., and Huang, H.W. (2013). Process of inducing pores in membranes by melittin. Proc. Natl. Acad. Sci. U S A *110*, 14243–14248.

Leive, L. (1965). Release of lipopolysaccharide by EDTA treatment of E. coli. Biochem. Biophys. Res. Commun. *21*, 290–296.

Leon-Buitimea, A., Garza-Cardenas, C.R., Garza-Cervantes, J.A., Lerma-Escalera, J.A., and Morones-Ramirez, J.R. (2020). The demand for new antibiotics: antimicrobial peptides, nanoparticles, and combinatorial therapies as future strategies in antibacterial agent design. Front. Microbiol. *11*, 1669.

Loike, J.D., and Silverstein, S.C. (1983). A fluorescence quenching technique using trypan blue to differentiate between attached and ingested glutaraldehyde-fixed red blood cells in phagocytosing murine macrophages. J. Immunol. Methods *57*, 373–379.

Macfarlane, E.L., Kwasnicka, A., Ochs, M.M., and Hancock, R.E. (1999). PhoP-PhoQ homologues in Pseudomonas aeruginosa regulate expression of the outer-membrane protein OprH and polymyxin B resistance. Mol. Microbiol. *34*, 305–316.

Martin, M. (2011). Cutadapt removes adapter sequences from high-throughput sequencing reads. EMBnet. J. *17*, 10–12.

McPhee, J.B., Lewenza, S., and Hancock, R.E. (2003). Cationic antimicrobial peptides activate a two-component regulatory system, PmrA-PmrB, that regulates resistance to polymyxin B and

cationic antimicrobial peptides in Pseudomonas aeruginosa. Mol. Microbiol. *50*, 205–217.

Mendez-Samperio, P. (2010). The human cathelicidin hCAP18/LL-37: a multifunctional peptide involved in mycobacterial infections. Peptides *31*, 1791–1798.

Michod, D., Annibaldi, A., Schaefer, S., Dapples, C., Rochat, B., and Widmann, C. (2009). Effect of RasGAP N2 fragment-derived peptide on tumor growth in mice. J. Natl. Cancer Inst. *101*, 828–832.

Michod, D., Yang, J.Y., Chen, J., Bonny, C., and Widmann, C. (2004). A RasGAP-derived cell permeable peptide potently enhances genotoxin-induced cytotoxicity in tumor cells. Oncogene *23*, 8971–8978.

Missiakas, D.M., and Schneewind, O. (2013). Growth and laboratory maintenance of Staphylococcus aureus. Curr. Protoc. Microbiol., Chapter 9, Unit 9C 1.

O'Neill, J. (2016). Tackling drug-resistant infections globally: final report and recommendations of the review on antimicrobial resistance. amr-review.org.

Ogasawara, H., Hasegawa, A., Kanda, E., Miki, T., Yamamoto, K., and Ishihama, A. (2007). Genomic SELEX search for target promoters under the control of the PhoQP-RstBA signal relay cascade. J. Bacteriol. *189*, 4791–4799.

Olaitan, A.O., Morand, S., and Rolain, J.M. (2014). Mechanisms of polymyxin resistance: acquired and intrinsic resistance in bacteria. Front. Microbiol. *5*, 643.

Pelletier, C., Bourlioux, P., and Van Heijenoort, J. (1994). Effects of sub-minimal inhibitory concentrations of EDTA on growth of Escherichia coli and the release of lipopolysaccharide. FEMS Microbiol. Lett. *117*, 203–206.

Pittet, O., Petermann, D., Michod, D., Krueger, T., Cheng, C., Ris, H.B., and Widmann, C. (2007). Effect of the TAT-RasGAP(317-326) peptide on apoptosis of human malignant mesothelioma cells and fibroblasts exposed to meso-tetra-hydroxyphenyl-chlorin and light. J. Photochem. Photobiol. B *88*, 29–35.

Rahme, L.G., Stevens, E.J., Wolfort, S.F., Shao, J., Tompkins, R.G., and Ausubel, F.M. (1995). Common virulence factors for bacterial pathogenicity in plants and animals. Science *268*, 1899–1902.

Robinson, M.D., McCarthy, D.J., and Smyth, G.K. (2010). edgeR: a Bioconductor package for differential expression analysis of digital gene expression data. Bioinformatics *26*, 139–140.

Sahlin, S., Hed, J., and Rundquist, I. (1983). Differentiation between attached and ingested immune complexes by a fluorescence quenching cytofluorometric assay. J. Immunol. Methods *60*, 115–124.

Schneider, C.A., Rasband, W.S., and Eliceiri, K.W. (2012). NIH Image to ImageJ: 25 years of image analysis. Nat. Methods *9*, 671–675.

Serulla, M., Ichim, G., Stojceski, F., Grasso, G., Afonin, S., Heulot, M., Schober, T., Roth, R., Godefroy, C., Milhiet, P.E., et al. (2020). TAT-RasGAP317-326 kills cells by targeting inner-leaflet-enriched phospholipids. Proc. Natl. Acad. Sci. U S A. *117*, 31871–31881.

Six, D.A., Carty, S.M., Guan, Z., and Raetz, C.R. (2008). Purification and mutagenesis of LpxL, the lauroyltransferase of Escherichia coli lipid A biosynthesis. Biochemistry *47*, 8623–8637.

Solaimanpour, S., Sarmiento, F., and Mrazek, J. (2015). Tn-seq explorer: a tool for analysis of high-throughput sequencing data of transposon mutant libraries. PLoS One *10*, e0126070.

Spohn, R., Daruka, L., Lazar, V., Martins, A., Vidovics, F., Grezal, G., Mehi, O., Kintses, B., Szamel, M., Jangir, P.K., et al. (2019). Integrated evolutionary analysis reveals antimicrobial peptides with limited resistance. Nat. Commun. *10*, 4538.

Srinivas, P., and Rivard, K. (2017). Polymyxin resistance in gram-negative pathogens. Curr. Infect Dis. Rep. *19*, 38.

The Gene Ontology, C. (2019). The gene ontology resource: 20 years and still GOing strong. Nucleic Acids Res. *47*, D330–D338.

Tsoutsou, P., Annibaldi, A., Viertl, D., Ollivier, J., Buchegger, F., Vozenin, M.C., Bourhis, J., Widmann, C., and Matzinger, O. (2017). TAT-RasGAP317-326 enhances radiosensitivity of human carcinoma cell lines in vitro and in vivo through promotion of delayed mitotic cell death. Radiat. Res. *187*, 562–569.

Velkov, T., Roberts, K.D., Nation, R.L., Thompson, P.E., and Li, J. (2013). Pharmacology of polymyxins: new insights into an 'old' class of antibiotics. Future Microbiol. *8*, 711–724.

Vitale, A., Pessi, G., Urfer, M., Locher, H.H., Zerbe, K., Obrecht, D., Robinson, J.A., and Eberl, L. (2020). Identification of genes required for resistance to peptidomimetic antibiotics by transposon sequencing. Front. Microbiol. *11*, 1681.

Wan, C.P., Park, C.S., and Lau, B.H. (1993). A rapid and simple microfluorometric phagocytosis assay. J. Immunol. Methods *162*, 1–7.

Wang, G., Li, X., and Wang, Z. (2016). APD3: the antimicrobial peptide database as a tool for research and education. Nucleic Acids Res. *44*, D1087–D1093.

Weatherspoon-Griffin, N., Yang, D., Kong, W., Hua, Z., and Shi, Y. (2014). The CpxR/CpxA two-component regulatory system up-regulates the multidrug resistance cascade to facilitate Escherichia coli resistance to a model antimicrobial peptide. J. Biol. Chem. *289*, 32571–32582.

Winsor, G.L., Griffiths, E.J., Lo, R., Dhillon, B.K., Shay, J.A., and Brinkman, F.S. (2016). Enhanced annotations and features for comparing thousands of Pseudomonas genomes in the Pseudomonas genome database. Nucleic Acids Res. *44*, D646–D653.

Xhindoli, D., Pacor, S., Benincasa, M., Scocchi, M., Gennaro, R., and Tossi, A. (2016). The human cathelicidin LL-37–A pore-forming antibacterial peptide and host-cell modulator. Biochim. Biophys. Acta *1858*, 546–566.

Yadavalli, S.S., Carey, J.N., Leibman, R.S., Chen, A.I., Stern, A.M., Roggiani, M., Lippa, A.M., and Goulian, M. (2016). Antimicrobial peptides trigger a division block in Escherichia coli through stimulation of a signalling system. Nat. Commun. *7*, 12340.

Yamamoto, N., Nakahigashi, K., Nakamichi, T., Yoshino, M., Takai, Y., Touda, Y., Furubayashi, A., Kinjyo, S., Dose, H., Hasegawa, M., et al. (2009). Update on the Keio collection of Escherichia coli single-gene deletion mutants. Mol. Syst. Biol. *5*, 335.

Yang, L., Harroun, T.A., Weiss, T.M., Ding, L., and Huang, H.W. (2001). Barrel-stave model or toroidal model? A case study on melittin pores. Biophys. J. *81*, 1475–1485.

Yethon, J.A., Heinrichs, D.E., Monteiro, M.A., Perry, M.B., and Whitfield, C. (1998). Involvement of waaY, waaQ, and waaP in the modification of Escherichia coli lipopolysaccharide and their role in the formation of a stable outer membrane. J. Biol. Chem. *273*, 26310–26316.

STAR★METHODS

KEY RESOURCES TABLE

REAGENT or RESOURCE	SOURCE	IDENTIFIER
Bacterial and virus strains		
Escherichia coli K-12 MG1655	ATCC	47076
Escherichia coli K-12 BW25113	Horizon Discovery, Cambridge, UK	OEC5042
Escherichia coli O6	ATCC	25922
Pseudomonas aeruginosa PA14	Isolated from burn wound (Rahme et al., 1995)	N/A
Staphylococcus capitis	Isolated from contaminated cell culture (Heulot et al., 2017)	N/A
Staphylococcus aureus subsp. *aureus* Rosenbach	ATCC	29213
Chemicals, peptides, and recombinant proteins		
TAT-RasGAP$_{317-326}$	SBS Genetech	Cat#2012-04-3
FITC-TAT-RasGAP$_{317-326}$	SBS Genetech	Cat#2012-04-4
Melittin	Enzo Life Science	Cat#ALX-162-006-M0005
Polymyxin B	Sigma-Aldrich	Cat#P4932
LL-37	Sigma-Aldrich	Cat#94261
FM4-64-FX	Molecular Probes	Cat#F34653
Paraformaldehyde (16% aqueous solution)	Electron Microscopy Sciences	Cat#15710
DAPI dilactate	Invitrogen	Cat#D3571
Lipopolysaccharide from *Escherichia coli* O55:B5	Sigma-Aldrich	Cat#L4524
EDTA	Fluka	Cat#03680
2.5% Glutaraldehyde in 0.1 M Phosphate Buffer, pH 7.4	Electron Microscopy Sciences	Cat#16537-05
Osmium tetroxide	Electron Microscopy Sciences	Cat#19100
Potassium ferrocyanide	Electron Microscopy Sciences	Cat#20150
Low melting agarose SFR	Electron Microscopy Sciences	Cat#10207
Acetone	Electron Microscopy Sciences	Cat#10000
Epon	Electron Microscopy Sciences	Cat#14910
Uranyl acetate	Electron Microscopy Sciences	Cat#22400
Trypan blue 0.4%	Gibco	Cat#15250-061
Lysozyme	AppliChem	Cat#A4972
L-rhamnose monohydrate	Sigma-Aldrich	Cat#R3875-25G
BamHI restriction enzyme	New England Biolabs	Cat#R3136S
Sodium Dodecyl-sulfate	Sigma-Aldrich	Cat#71729
Critical commercial assays		
RNeasy Plus Mini Kit	Qiagen	Cat#74134
DNA-free™ DNA Removal Kit	Invitrogen	Cat#AM1906
Standard Sensitivity RNA Analysis kit	Agilent Technologies	Cat# DNF-471-0500
GenElute Bacterial Genomic DNA Kit	Sigma-Aldrich	Cat#NA2110
NEBNext Ultra II DNA Library Prep Kit	New England Biolabs	Cat#E7645S
MiSeq Reagent Kit v2	Illumina	Cat#MS-102-2002

(*Continued on next page*)

Continued

REAGENT or RESOURCE	SOURCE	IDENTIFIER
Deposited data		
RNA-seq Data	This study	https://www.ebi.ac.uk/ena/browser/view/PRJEB45735
Transposon sequencing Data	This study	https://www.ebi.ac.uk/ena/browser/view/PRJEB45735
Oligonucleotides		
Transposon amplification		
T23_SLXA_PAIR_Amp	AATGATACGGCGACCACCGAGATCTA CACTAGAGAATAGGAACTTCGGAAT AGGAACTTCTTAGATGTGTATAAGAG	(Higgins et al., 2017)
SLXA_PAIR_REV_AMP	CAAGCAGAAGACGGCATACGAGATCG GTCTCGGCATTCCTGCTGAACCGCTCT TCCGATCT	(Higgins et al., 2017)
Sequencing		
T23_SEQ_G	ATTAGGAACTTCGGAATAGGAACTTC TTAGATGTGTATAAGAGACAG	(Higgins et al., 2017)
T23_INDEX_1	CTAGAGAATAGGAACTTCGGAATAGG AACTTCTTAGATGTGTATAAG	(Higgins et al., 2017)
PE_READ2_SEQ	CGGTCTCGGCATTCCTGCTGAACCGC TCTTCCGATCT	(Higgins et al., 2017)
Software and algorithms		
Image J	Schneider et al., 2012	https://imagej.nih.gov/ij/
Prism 8	GraphPad	N/A
Tn-Seq explorer	Solaimanpour et al., 2015	http://www.cmbl.uga.edu/downloads/programs/Tn_seq_Explorer/
Keio collection screening analysis	This study	https://github.com/njacquie/TAT-RasGAP_project

RESOURCE AVAILABILITY

Lead contact

Further information and requests for resources and reagents should be directed to and will be fulfilled by the lead contact, Nicolas Jacquier (nicolas.jacquier@chuv.ch).

Materials availability

Bacterial strains generated during this study are available from the lead contact upon request.

Data and code availability

- RNA-seq data have been deposited to European Nucleotide Archive (ENA) under the project accession number [ENA]:[PRJEB45735] and are publicly available as of the date of publication. Accession numbers are listed in the key resources table. Other raw data will be shared by the lead contact upon request.
- All original code has been deposited on Github (https://github.com/njacquie/TAT-RasGAP_project). as detailed in the key resources table and is publicly available as of the date of publication.
- Any additional information required to reanalyze the data reported in this paper is available from the lead contact upon request.

EXPERIMENTAL MODELS AND SUBJECT DETAILS

Escherichia coli K-12 MG1655, ATCC47076.

Escherichia coli K-12 BW25113, wild-type strain from the Keio deletion mutants collection, purchased through Horizon Discovery, Cambridge, UK.

Escherichia coli O6 ATCC25922.

Pseudomonas aeruginosa PA14, clinical isolate from burn wound (Rahme et al., 1995).

All *E. coli* and *P aeruginosa* strains were grown in LB medium (10 g/L tryptone, 5g/L Yeast extract, 10g/L NaCl) BD 244620 at 37°C or Basal Medium 2 (BM2; 62 mM potassium phosphate buffer [pH 7.0], 7 mM $(NH_4)_2SO_4$, 10 μM $FeSO_4$, 0.4% (wt/v) glucose and 0.5% tryptone) with high (2 mM) or low (20 μM) concentration of magnesium ($MgSO_4$) (Fernandez et al., 2012).

Staphylococcus capitis, strain isolated as a culture contaminant (Heulot et al., 2017).

Staphylococcus aureus subsp. *aureus* Rosenbach ATCC 29213.

Staphylococcus strains were grown in tryptic soy broth (TSB) (Missiakas and Schneewind, 2013).

All strains were stored at -80°C, in their respective medium, supplemented with ~25% glycerol.

METHOD DETAILS

TAT-RasGAP$_{317-326}$ peptide

The retro-inverse TAT-RasGAP$_{317-326}$ peptide (amino acid sequence DTRLNTVWMWGGRRRQRRKKRG) and the N-terminal FITC-labeled version of this peptide were synthesized by SBS Genetech (Beijing, China) and stored at -20°C.

MIC measurements

The minimum inhibitory concentration (MIC) of peptide was defined as the lowest concentration of peptide that resulted in no visible growth. Overnight cultures were diluted to OD_{600} = 0.1 and grown with shaking at 37°C for 1 hour. MICs were measured by diluting these cultures (1:20 for LB and TSB cultures and 1:8 for BM2 cultures) and then adding these dilutions to 2-fold sequential dilutions of the peptides in 96-well plates. Volume of media (with peptide) per well was 100 μl and 10 μl of diluted cultures were added to each well. Cell growth was monitored via OD_{590} measurement after overnight growth at 37°C. OD_{590} readings were measured by FLUOstar Omega microplate reader (BMG Labtech, Ortenberg, Germany). Peptide-free growth control wells and bacteria-free contamination control wells were included. First concentration at which no bacterial growth could be detected was defined as the MIC.

For MIC measurements in presence of *E. coli* LPS or EDTA, the indicated concentrations of these substances were dissolved in LB and distributed in 96-well plates prior to addition of the peptides. OD_{590} measurements of control wells without peptides were used to calculate the percentage of growth in presence of EDTA.

Growth curves

Overnight cultures were diluted to OD_{600} = 0.1 and grown with shaking at 37°C for 1 hour, before addition of peptide. Cell growth was monitored via OD_{600} measurement by Novaspec II Visible spectrophotometer (Pharmacia LKB Biotechnology, Cambridge, England) at 2, 4 and 6 hours. Combinations of antimicrobial peptides were tested using the above methods and combining "half" concentrations of the different peptides (2 μM TAT-RasGAP$_{317-326}$, 64 μg/ml melittin, 32 μg/ml LL-37 or 1 μg/ml polymyxin B) to produce Figure S8C.

CFU measurements

Overnight cultures were diluted to OD_{600} = 0.1 and grown with shaking at 37°C for 1 hour, before addition of the peptide. Each time point was taken by removing 10 μl and performing 10-fold serial dilutions. Dilutions of each condition were then plated in the absence of peptide and grown at 37°C overnight. CFU were measured by counting the number of colonies on the plates after overnight incubation.

Confocal microscopy

Overnight cultures of *E. coli* MG1655 were diluted to OD_{600} = 0.1, grown for 1 hour, incubated for 1 hour with 10 μM FITC-labeled TAT-$RasGAP_{317-326}$, stained with 5 μg/ml FM4-64 and fixed with 4% paraformaldehyde solution. Incubation with DAPI was subsequently performed and pictures were acquired on a LSM710 confocal microscope (Zeiss, Oberkochen, Germany). Images were analyzed with ImageJ software (Schneider et al., 2012).

Electron microscopy

Bacteria were fixed with 2.5% glutaraldehyde solution (EMS, Hatfield, PA) in Phosphate Buffer (PB 0.1 M pH 7.4) for 1 hour at room temperature. Then, bacterial samples were incubated in a freshly prepared mix of 1% osmium tetroxide (EMS) and 1.5% potassium ferrocyanide in phosphate buffer for 1 hour at room temperature. The samples were then washed three times in distilled water and spun down in 2% low melting agarose, solidified on ice, cut into 1 mm^3 cubes and dehydrated in acetone solution at graded concentrations (30% for 40 minutes; 50% for 40 minutes; 70% for 40 minutes and 100% for 3 times 1 hour). This was followed by infiltration in Epon at graded concentrations (Epon 1/3 acetone for 2 hours; Epon 3/1 acetone for 2 hours, Epon 1/1 for 4 hours and Epon 1/1 for 12 hours) and finally polymerization for 48 hours at 60°C in a laboratory oven. Ultrathin sections of 50 nm were cut on a Leica Ultramicrotome (Leica Mikrosysteme GmbH, Vienna, Austria) and placed on a copper slot grid 2x1mm (EMS) coated with a polystyrene film. The bacterial sections were stained in 4% uranyl acetate for 10 minutes, rinsed several times with water, then incubated in Reynolds lead citrate and finally rinsed several times with water before imaging.

Micrographs (10x10 tiles) with a pixel size of 1.209 nm over an area of 40x40 μm were taken with a transmission electron microscope Philips CM100 (Thermo Fisher Scientific, Waltham, MA) at an acceleration voltage of 80kV with a TVIPS TemCam-F416 digital camera (TVIPS GmbH, Gauting, Germany). Large montage alignments were performed using Blendmont command-line program from the IMOD software (Kremer et al., 1996) and treated with ImageJ software.

Flow cytometry

Overnight cultures of *E. coli* MG1655 were diluted 1:100 and grown to mid exponential phase (OD_{600} = 0.4-0.6) with shaking at 37°C. Each culture was then diluted to OD_{600} = 0.1, grown with shaking at 37°C for 1 hour and then treated with 10 μM FITC-labeled peptide for 1 hour. Following peptide treatment, bacterial cells were washed in PBS and diluted 1:5 before acquisition on a CytoFLEX benchtop flow cytometer (Beckman Coulter). For each sample, 10,000 events were collected and analyzed. Extracellular fluorescence was quenched with 0.2% Trypan Blue (TB). TB is an efficient quencher of extracellular fluorescence (Sahlin et al., 1983; Loike and Silverstein, 1983; Jevprasesphant et al., 2004; Wan et al., 1993) and allows quantification of fluorescent signal from intracellular peptide (not subject to quenching by TB). P values were calculated using ratio paired t-test.

RNA-Seq

Overnight cultures of *E. coli* MG1655 were diluted to OD_{600} = 0.1 and grown with shaking at 37°C for one hour to mid exponential phase (OD_{600} = 0.4-0.6). Cultures were then treated with TAT-$RasGAP_{317-326}$ (10 μM) or left untreated (negative control), and grown with shaking at 37°C for an additional hour. For RNA extraction, protocol 1 in the RNAprotect Bacteria Reagent Handbook (Enzymatic lysis of bacteria) was followed using the RNeasy Plus Mini Kit (Qiagen) using TE buffer (10 mM Tris-HCl, 1 mM EDTA, pH 8.0) containing 1 mg/ml lysozyme (AppliChem, Chicago, IL). In the last step, RNA was eluted in 30 μl RNase-free water. Next, any contaminating DNA was removed using the DNA-free™ DNA Removal Kit (Invitrogen, Carlsbad, CA). 10x DNase buffer was added to the 30 μl eluted RNA with 2 μl rDNase I. This mix was incubated for 30 minutes at 37°C followed by rDNase I inactivation with 7 μl DNase Inactivation Reagent for 2 minutes with shaking (700 rpm) at room temperature. Samples were then centrifuged for 90 seconds at 10,000 x *g*, supernatant was transferred to a new tube, and stored at -80°C. Integrity of the samples was verified using the Standard Sensitivity RNA Analysis kit (Advanced Analytical, Ankeny, IA) with the Fragment Analyzer Automated CE System (Labgene Scientific, Châtel-Saint-Denis, Switzerland). Samples that met RNA-Seq requirements were further processed and sent for sequencing. Preparation of the libraries and Illumina HiSeq platform (1x50 bp) sequencing were performed by Fasteris (Plan-les-Ouates, Switzerland). Raw reads were trimmed with trimmomatic version 0.36 (Bolger et al., 2014) (parameters: ILLUMINACLIP: NexteraPE-PE.fa:3:25:6, LEADING: 28, TRAILING: 28 MINLEN: 30). Trimmed reads were mapped to the genome of *E. coli* K-12 MG1655 (accession: NC_000913.3) with bwa mem version 0.7.17

(https://arxiv.org/abs/1303.3997) using default parameters. Htseq version 0.11.2 (Anders et al., 2015) was used to count reads aligned to each gene (parameters: –stranded=no -t gene). Normalized expression values were calculated as Reads Per Kilobase of transcript per Million mapped reads (RPKM) with edgeR (Robinson et al., 2010).

Keio collection screening

Deletion mutants from the Keio collection (Baba et al., 2006; Yamamoto et al., 2009) were used, along with the corresponding wild-type, which was added as a control on each test plate. Overnight cultures were diluted 1:100 in LB medium. Bacteria were incubated at 37°C for 1 hour before adding TAT-RasGAP$_{317\text{-}326}$ (5 μM final concentration). Plates were incubated statically at 37°C and OD_{590} was measured at 0, 1.5 hour, 3 hours, 6 hours and 24 hours with FLUOstar Omega plate reader. Measurements were combined and analyzed with R (version 3.6.1, https://www.r-project.org/). Data analysis and visualization were performed with the *dplyr* (version 0.8.5) and *ggplot2* (version 3.3.0) packages from the *tidyverse* (version 1.3.0) environment. Since starting OD_{590} (OD in equations) varied between strains and conditions, the OD_{590} starting values in each well was subtracted from corresponding measurements made at time t in the presence (P) or absence (noP) of TAT-RasGAP$_{317\text{-}326}$. For each strain, $NG^m_t(P)$, the normalized growth value for a mutant strain at time t in the presence of the peptide was calculated with the following formula:

$$NG_t^m(P) = \frac{OD_t^m(P) - OD_0^m(P)}{OD_t^m(noP) - OD_0^m(noP)}$$

Normalized growths of wild-type strain (mean WT), as presented on Figures 4A and 4B were calculated by averaging normalized growths of all the wild-type controls performed (N=270).

To normalize the growth of a mutant (m) to the growth of control (c) bacteria (wild-type) on the same plate, the $NG^m_t(noP)$ factor was calculated with the following formula:

$$NG_t^m(noP) = \frac{OD_t^m(noP) - OD_0^m(noP)}{OD_t^c(noP) - OD_0^c(noP)}$$

Gene ontology (GO) annotation (The Gene Ontology, 2019) was obtained from GO database (2020-09-01, "http://current.geneontology.org/annotations") and assigned to the list of gene deletion inducing hypersensitivity with the GO.db package (version 3.10.0 (Carslon, 2019)). GO IDs were assigned to each gene and the corresponding GO names were obtained with the "Term" function. Additionally, the same set of genes was subjected to KEGG pathways analysis (Kanehisa and Goto, 2000) with the KEGGREST package (version 1.26.1). Briefly, the KEGG orthology (KO) and KEGG pathway annotation were obtained from the KEGG database (Kanehisa, 2019) for *E. coli* K-12 MG1655 (eco).

Pseudomonas aeruginosa PA14 transposon library screening

The library of transposon (Tn) mutants in *P. aeruginosa* PA14 (Vitale et al., 2020) was grown in BM2 supplemented with 20 μM $MgSO_4$ (Fernandez et al., 2012) and 0.2% L-rhamnose monohydrate (Sigma-Aldrich) in the absence or presence of 0.5 μM TAT-RasGAP$_{317\text{-}326}$. Following growth for 12 generations, genomic DNA (gDNA) was extracted with the GenElute Bacterial Genomic DNA Kit (Sigma-Aldrich). The transposon sequencing (Tn-seq) circle method (Gallagher et al., 2011, 2013) was employed to sequence the transposon junctions. Briefly, the gDNA was sheared to an average size of 300 bp fragments with a focused-ultrasonicator. The DNA fragments were repaired and ligated to adapters with the NEBNext Ultra II DNA Library Prep Kit for Illumina (New England Biolabs). Following restriction of the Tn with BamHI (New England Biolabs), the fragments were circularized by ligation and exonuclease treatment was applied to remove undesired non-circularized DNAs (Gallagher et al., 2011). The Tn junctions were PCR amplified and amplicons were sequenced with the MiSeq Reagent Kit v2, 300-cycles (Illumina) (Higgins et al., 2017).

Following sequencing, the adapter sequences of the reads (.fastq) were trimmed with the command line "cutadapt -a adapter -q quality -o output.fastq.gz input.fastq.gz" (Martin, 2011). The software Tn-Seq Explorer (Solaimanpour et al., 2015) mapped the trimmed and paired reads onto the *P. aeruginosa* UCBPP-PA14 genome (Winsor et al., 2016), and determined the unique insertion density (UID, i.e. the number of unique Tn insertions divided per the length of the gene). The normalized UID between the treated and non-treated samples were compared and this ratio (log2-fold change, FC) was used to identify resistant determinants (log2-FC < - 1.0 and normalized UID > 0.0045).

Selection of resistant mutants

Bacteria were grown in the corresponding medium, diluted 1:100 and cultured overnight with 0.5x MIC of TAT-RasGAP$_{317-326}$. The subculture was diluted 1:100 and incubated with 0.5x or 1x MIC overnight. Cells that successfully grew were diluted 1:100 in medium containing the same concentration or increased concentration of peptide. Each dilution in fresh medium containing peptide is considered one passage. This process was repeated for up to 20 passages.

QUANTIFICATION AND STATISTICAL ANALYSIS

Quantifications and statistical analyses were performed using GraphPad Prism 8 software. Method of analysis and number of replicates are mentioned in the figure legends.